Chapter 5: Computational Approaches to Polymeric Nanocomposites

S. O. Ojo [a, *], S. O. Ismail [b]

[a] Bernal Institute, School of Engineering, University of Limerick, Castletroy, V94 T9PX, Ireland

[b] Centre for Engineering Research, Department of Engineering, School of Physics, Engineering and Computer Science, University of Hertfordshire, AL10 9AB, England, UK

*_Corresponding author_: S. O. Ojo, E-mail: saheed.ojo@ul.ie, Tel. No: +353 871660854

Abstract

Understanding hierarchical structures and behaviours of polymeric nanocomposites (PNCs) is essential to achieve optimum improvement in the properties of PNCs for a wide range of applications. To control the process of material synthesis, it is vital to employ computational strategies that can accurately predict the properties of candidate materials. Therefore, this chapter reviews the computational approaches to predicting the behaviours of PNCs. A general approach to modelling the physical and mechanical properties of PNCs in terms of analytical and numerical techniques is first presented, with a view to understand modelling approaches at different levels of complexities, lengths, and time scales, such as molecular, microscale, mesoscale, and macroscale. Then, specific attention is given to multiscale hierarchical modelling of PNCs to highlight techniques to bridge the gap between numerical and analytical models at different scales. This chapter further considers various aspects of emerging applications of single scale and multiscale numerical techniques to nanostructure systems. Lastly, it discusses current challenges encountered in the application of computational methods to improve the performance of polymeric nanomaterials in line with future prospects, prior to the concluding remarks.

Keywords: Polymeric nanocomposites (PNCs), computational approaches, physical properties, mechanical properties, multiscale modelling.

Nomenclature

BD	Brownian dynamics
CM	continuum mechanics
CNT	carbon nanotube

DFT	density functional theory
DPD	dissipative particle dynamics
EC	Equivalent continuum
EMA	effective medium approximation/approach
FEM	finite element method
HT	Halpin-Tsai
LB	lattice Boltzmann
MC	Monte Carlo
MD	molecular dynamics
MM	molecular mechanics
MMT	montmorillonite
MR	material region
MSFEM	multiscale finite element method
MT	Mori-Tanaka
PDF	Probability distribution function
PEO	poly (ethylene oxide)
PNCs	polymeric nanocomposites
ROM	rule of mixtures
RVE	representative volume element
SERVE	statistically equivalent representative volume element
SVE	statistical volume element
SWCNT	single-walled carbon nanotube

5.0 Introduction

The emergence of nanocomposites as a new class of materials has triggered interest in their development and applications in the last few decades. The unique properties of nanoparticles when introduced into continuous polymer matrix have resulted into new phenomena and exceptional properties with promising applications in engineering industries, such as automotive, packaging, and medical devices. For specific applications, prediction of properties is necessary for efficient design and synthesis of new materials. However, the poor understanding of fundamental issues bordering on prediction of nanoparticle structure (specifically, the effects of nanofiller size and architecture on the nanocomposite morphology), dynamics (that is, the effect of nanofillers on the rheological characteristics of the melt), solid-

state properties, and processing methods and conditions constitute challenges hindering further developments in the field of nanocomposites.

To a large extent, the quality of dispersion of nanoscale fillers in the polymer matrix significantly affects the final properties of polymeric nanocomposites (PNCs), yet it is challenging to achieve optimal dispersion of nanoparticles owing to their tendency to form nanoparticle aggregates and platelet stacks or due to uncertainties in the properties of nanoparticles and dissimilarity between the chemical properties of matrix and nanofillers [1].

In light of these observations, the experimental approach creates some challenges, which limit the ability to characterise the structure and control the process of fabricating PNCs. Therefore, for efficient design of polymeric nanocomposite (PNC) materials, predictive tools which can sufficiently capture these nanoscale phenomena must be employed to guide material synthesis. Fundamentally, predictive models address issues, including thermodynamics and kinetics formation of PNCs; the effect of nanoparticles on the polymer rheological behaviour; hierarchical features of the structure and dynamics of PNCs from the molecular scale to the macroscale; and the reinforcement mechanisms of nanoparticles in PNCs [2]. Furthermore, modelling of nanocomposite properties is essential to eliminate the need to synthesise each and every composite to determine their properties. Practically, predictive models use realistic assumptions that are capable of accurately and efficiently simulating experimental observations in the nanoscale to generate information needed for design purposes in the macroscale. From the multiscale perspective, computational approach to modelling PNCs involves three procedures depending on the structural level [2]:

- *Molecular scale methods*: These refer to modelling and simulation methods which employ atoms, molecules, or their clusters as the basic unit of the simulation cell. Popular methods in this category include Monte Carlo (MC) and Molecular dynamics (MD) methods.
- *Microscale methods*: These represent modelling methods which combine the merits of molecular and continuum methods to investigate the microscopic structure and phase separation of PNCs. Examples in this context include dissipative particle dynamics (DPD), dynamic density functional theory (DDFT), lattice Boltzmann (LB), Brownian dynamics (BD), and time-dependent Ginzburg-Lanau method.
- *Mesoscale and macroscale methods*: These are methods which rely on the fundamental laws of equilibrium together with the laws of conservation of energy, mass, moment, and

entropy to describe the mesoscale and macroscopic behaviours of PNC structure represented by an equivalent continuum material. Examples include micromechanics, finite element method, equivalent-continuum, and self-similar approaches.

These methods are generally classified into analytical and numerical methods and are applicable at different length and time scales and at different levels of complexity.

5.1 Analytical methods

For some simplified structures, analytical models give satisfactory outcomes in terms of accuracy, computational efficiency, and predictive capacity. Analytical methods rely on micromechanical approach by using a representative volume element (RVE) to statistically describe the local continuum properties [1]. In this context, the properties of the nanocomposite can be determined based on the properties of the constituents and their volume fractions or geometry of the reinforcements and their dispersion characteristics in the matrix. Some examples of micromechanical analytical models include the Einstein [3], rule of mixtures, cox (shear-lag), Halpin-Tsai, Nielson as well as Mori-Tanaka models [1]. For didactic purpose, this chapter will focus on analytical methods for the prediction of mechanical and thermal properties of PNCs.

5.1.1 Mechanical Properties

5.1.1.1 Rule of Mixtures

Rule of mixtures (ROM) is the simplest approach to predict the properties of composites. The basic assumption in this approach is that the properties of composites are dependent on the volume fraction of the constituent phases in the composite. Essentially, the properties of the filler and matrix constituents are used to estimate the macroscopic properties of composites [1].

In line with the Voigt's isostrain assumption, specifically the strain parallel to continuous parallel fibre must be equal in both filler and matrix components of the fibre, the longitudinal modulus, E_{11} of a composite with aligned continuous fillers is expressed as Equation (5.1) [4].

$$E_{11} = E_f V_f + E_m V_m \tag{5.1}$$

where E_f and E_m represent the moduli of fibre and matrix respectively, while V_f and V_m denote the volume fractions of fibre and matrix respectively. Conversely, the transverse modulus, E_{22} is determined according to Reuss's assumption in which transverse stress in the filler and the matrix is considered to be equal, leading to Equation (5.2) [4].

$$\frac{1}{E_{22}} = \frac{V_f}{E_f} + \frac{V_m}{E_m} \tag{5.2}$$

Similarly, the in-plane shear modulus, G_{12} can be derived according to the equal stress assumption, that is:

$$\frac{1}{G_{12}} = \frac{V_f}{G_f} + \frac{V_m}{G_m} \tag{5.3}$$

where G_f and G_m are shear moduli of the fibre and matrix, respectively. In case the matrix is filled with randomly distributed fillers, the elastic and shear moduli of the nanocomposite are approximated as Equations (5.4) and (5.5), respectively [4].

$$E_c = \frac{3}{8}E_{11} + \frac{5}{8}E_{22} \tag{5.4}$$

$$G_c = \frac{1}{8}E_{11} + \frac{1}{4}E_{22} \tag{5.5}$$

It is noted that other properties of the composite can be predicted by the ROM theory as summarised and presented in Table 5.1 [1].

Table 5.1: Rule of mixture formula for property prediction of composite materials

Property	**Equation**
Density (ρ)	$\rho = \rho_f V_f + \rho_m V_m$
Average stress ($\bar{\sigma}$)	$\bar{\sigma} = \bar{\sigma}_f V_f + \bar{\sigma}_m V_m$
Average strain ($\bar{\varepsilon}$)	$\bar{\varepsilon} = \bar{\varepsilon}_f V_f + \bar{\varepsilon}_m V_m$
Poisson's ratio (υ)	$\upsilon = \upsilon_f V_f + \upsilon_m V_m$
Thermal conductivity (κ)	$\kappa = \kappa_f V_f + \kappa_m V_m$
Thermal expansion coefficient (α)	$\alpha = \alpha_f V_f + \alpha_m V_m$
Electrical conductivity (μ)	$\mu = \mu_f V_f + \mu_m V_m$
Gas diffusivity (D)	$D = D_f V_f + D_m V_m$

The subscripts, f and m refer to filler (fibre) and matrix, respectively. Overbar terms refer to average values.

Due to the isostrain condition, the fibres fail before the matrix reaches its tensile strength. Thus, the ROM model is inadequate to predict the strength of unidirectional composites [5]. In addition, ROM theory neglects the effect of the filler orientation and size in its estimate, leading to inaccuracies in the predictions.

5.1.1.2 Halpin-Tsai Model

The Halpin-Tsai (HT) model is a semi-empirical method that predicts the stiffness of unidirectional composites based on the geometry and the orientation of the filler and the elastic properties of filler and matrix. The general form of the longitudinal, E_{11} and transverse, E_{22} moduli is expressed as Equation (5.6) [4, 6].

$$\frac{E_i}{E_m} = \frac{1+\eta_i \xi_i V_f}{1-\eta_i V_f} \tag{5.6}$$

where η_i is expressed as [4]

$$\eta_i = \frac{E_f/E_m - 1}{E_f/E_m + \xi_i} \qquad i = 11, 22 \tag{5.7}$$

The shear modulus, G_{12} can be determined as Equation (5.8) [4].

$$\frac{G_{12}}{G_m} = \frac{1}{1-\eta_{12} V_f} \tag{5.8}$$

where η_{12} is expressed as [4]

$$\eta_{12} = \frac{G_f/G_m - 1}{G_f/G_m} \tag{5.9}$$

In Equations (5.6-5.9), E_f and E_m are the Young's moduli of the filler and the matrix respectively, while G_f and G_m correspond to the shear moduli of the fibre and matrix, respectively. In addition, V_f is the filler volume fraction and ξ is a geometry parameter, that is a measure of reinforcement geometry, packing geometry and loading conditions, and is expressed for a rectangular-shaped (for example, platelets or lamellar-shaped) filler in the longitudinal and transverse directions, respectively, as:

$$\xi_{11} = \frac{2l}{t} \tag{5.10}$$

$$\xi_{22} = \frac{2w}{t} \tag{5.11}$$

where l, w and t are the filler length, width, and diameter, respectively. In the case of cylindrical-shaped filler with diameter, $d = t = w$, the reinforcement parameters in the longitudinal and transverse directions become $\xi_{11} = \frac{2l}{d}$ and $\xi_{22} = 2$, respectively. The classical HT mathematical model is not suitable for composites reinforced with more than one scale of reinforcements, for example, composites reinforced with randomly oriented fibres. In this regard, the modified HT model for elastic modulus of composite with randomly oriented fibres, E_c, takes the form of Equation (5.12) [4].

$$\frac{E_c}{E_m} = \frac{3}{8}\left(\frac{1+\eta_L \xi V_f}{1-\eta_L V_f}\right) + \frac{5}{8}\left(\frac{1+2\eta_T V_f}{1-\eta_T V_f}\right) \tag{5.12}$$

where η_L and η_T, respectively, are expressed as [4]

$$\eta_L = \frac{E_f/E_m - 1}{E_f/E_m + 2l/d} \tag{5.13}$$

$$\eta_T = \frac{E_f/E_m - 1}{E_f/E_m + 2} \tag{5.14}$$

5.1.1.3 Mori-Tanaka Model

The Mori-Tanaka (MT) model is commonly used to model the behaviour of particle reinforced composites in which the elastic modulus and the Poisson's ratio are expressed as Equations (5.15) and (5.16), respectively [4].

$$E_c = \frac{9K_c G_c}{3K_c + G_c} \tag{5.15}$$

$$\nu_c = \frac{3K_c - 2G_c}{6K_c + 2G_c} \tag{5.16}$$

where K_c and G_c are the bulk and shear moduli of the composites respectively, which are further expressed as Equations (5.17) and (5.18), respectively [4].

$$K_c = K_m + \frac{V_f(K_f - K_m)}{1 + (1 - V_f)[3(K_f - K_m)/(3K_m + 4G_m)]} \tag{5.17}$$

$$G_c = G_m + \frac{V_f(G_f - G_m)}{1 + (1 - V_f)[(G_f - G_m)/(G_f + f_m)]} \tag{5.18}$$

in which

$$K_m = \frac{E_m}{3(1-2\nu_m)},\ K_f = \frac{E_f}{3(1-2\nu_f)},\ G_m = \frac{E_m}{2(1+\nu_m)},\ G_f = \frac{E_f}{2(1+\nu_f)},\ f_m = \frac{G_m(9K_m + 8G_m)}{6(K_m + 2G_m)}$$

A common phenomenon in particle reinforced composites is the agglomeration of fillers to form inclusion-like constituents. In this regard, to predict an elastic field in and around a spherical inclusion in an isotropic matrix, a modified MT model which combines MT theory with the principle of Eshelby's inclusion was proposed by Tandon and Weng [7], with analytical expression for the longitudinal and transverse moduli, given as Equations (5.19) and (5.20), respectively [4].

$$\frac{E_{11}}{E_m} = \frac{A_0}{A_0 + V_f(A_1 + 2v_m A_2)} \tag{5.19}$$

$$\frac{E_{22}}{E_m} = \frac{2A_0}{2A_0 + V_f[-2v_m A_3 + (1 - v_m)A_4 + (1 + v_m)A_0 A_5]} \tag{5.20}$$

where v_m represents the Poisson's ratio of the matrix and the parameters, $A_0, \ldots, A_5$, which depend on the Eshelby's tensor as well as the properties of the filler and the matrix, are given in [7].

5.1.2 Thermal Properties

For applications that involve thermal insulation of materials, polymer processing, smart coatings, or thermoelectric devices, modelling of thermal conductivity of PNCs is important, since the polymer composites may contain pores, metals, carbon materials, ceramics, and semiconductors [8]. In general, four approaches can be used to model the effective thermal conductivity of PNCs: (i) micromechanical analogy, (ii) effective medium approximation (EMA), (iii) numerical methods and (iv) statistical approach. This section focuses on EMA and micromechanical analogy since they are analytical-based.

5.1.2.1 Micromechanical Approach

In the micromechanical approach, thermal conductivity is considered analogous with elastic stiffness or elastic shear modulus such that the flux field disturbance becomes analogous to stress field disturbance by the dispersed filler. For highly conductive particles, such as carbon nanotubes (CNT), the thermal conductivities of the resulting PNC exhibit significant disparity with the prediction obtainable by ROM [9]. Reasons for such discrepancies could be misalignment of CNTs, waviness of CNT shapes, CNT/matrix interfacial thermal resistance, void formation in CNT-based nanocomposites or lattice defects in CNT structure [10]. To explore the effect of these factors, thermal conductivity models presented in this section focus

on CNT-based nanocomposites, but the principle also applies to other highly conductive particles.

Classically, to estimate the axial thermal conductivity of an aligned straight CNT-reinforced nanocomposite considering the CNT volume fraction, length, and diameter, micromechanical analogy of elastic stiffness is extended to thermal conductivity to produce semi-empirical HT formula [11]:

$$\kappa = \kappa_m \left(\frac{1+\alpha\beta V_{\mathrm{CNT}}}{1-\beta\vartheta V_{\mathrm{CNT}}}\right) \tag{5.21}$$

where the parameters α, β and ϑ are expressed in Equations (5.22), (5.23) and (5.24) as:

$$\alpha = \frac{2l}{d} \tag{5.22}$$

$$\beta = \frac{\kappa_{\mathrm{CNT}}/K_{\mathrm{m}}-1}{\kappa_{\mathrm{CNT}}/K_{\mathrm{m}}+\alpha} \tag{5.23}$$

$$\vartheta = 1 + V_{\mathrm{CNT}} \left(\frac{1-\vartheta_m}{\vartheta_m^2}\right) \tag{5.24}$$

where κ_{m} and κ_{CNT} are the thermal conductivities of matrix and CNT, respectively. The terms l, d and V_{CNT} denote length, diameter, and volume fraction of the CNT, respectively. It is noted that, CNT/polymer interface plays a key role in the prediction of thermal conductivities of CNT-based nanocomposite due to large surface area-to-volume ratio of CNTs. For a more realistic prediction of thermal conductivity of CNT-based PNC, CNT/polymer interfacial thermal resistance, random orientation, CNT alignment, CNT waviness should be accounted for, in addition to CNT volume fraction, length and diameter. For example, the effect of interfacial thermal resistance can be incorporated into Equation (5.21) by considering the effective CNT thermal conductivity, which assumes interfacial thermal barrier as an equivalent nanofibre based on the simple rule of mixture [11]:

$$\kappa_{\mathrm{CNT}}^{\mathrm{eff}} = \frac{\kappa_{\mathrm{CNT}}}{1+2\kappa_{\mathrm{CNT}} r_k/(\kappa_{\mathrm{m}} L)}, \qquad r_k = R_k \kappa_{\mathrm{m}} \tag{5.25}$$

where r_k and R_k are the Kapitza radius and resistance, respectively. In addition, factors for CNT alignment, waviness and random orientation can be included in the model through the expression [11]:

$$\beta = \frac{\gamma\delta\varrho\kappa_{\mathrm{CNT}}/\kappa_{\mathrm{m}}-1}{\gamma\delta\varrho\kappa_{\mathrm{CNT}}/\kappa_{\mathrm{m}}+\alpha}, \quad \delta = 1 - \frac{A}{W} \tag{5.26}$$

where γ is the CNT alignment factor, δ is the waviness efficiency factor and ϱ is the orientation factor, whereas A and W are the amplitude and half wavelength of a wavy CNT, respectively. In some cases, an aggregated state for CNT into the polymer matrix may be observed, due to the PNC fabrication process. Therefore, an aggregation efficiency factor can further be included in Equation (5.27) [11].

$$\beta = \frac{\gamma\delta\varrho\varphi\kappa_{\mathrm{CNT}}/\kappa_{\mathrm{m}}-1}{\gamma\delta\varrho\varphi\kappa_{\mathrm{CNT}}/\kappa_{\mathrm{m}}+\alpha}, \quad \varphi = \exp(-V_{\mathrm{CNT}}^{\varepsilon}) \tag{5.27}$$

where ε relates to the CNT aggregation degree, which depends on the fabrication process of the CNT-based nanocomposites.

In general, the choice of micromechanical model for good prediction of thermal conductivity depends on the degree of filler loading, nature of interface (specifically, interfacial resistance), shape and size of inclusions and filler distribution [10]. Therefore, for accurate thermal conductivity predictions, accurate input parameters must be supplied to the analytical models. One way to improve the accuracy of the predictions is the combination of numerical and analytical approaches. For example, in a study [9], atomistic MD simulations can be used to determine the interfacial thermal resistance between the nanoparticles and the polymer hydrocarbon chains, while analytical approach is adopted to estimate the thermal conductivity, using the calculated resistance from MD simulation. Other examples of analytical models which can be applied for specific conditions of filler qualities are presented in Table 5.2.

Table 5.2: Micromechanical-based thermal models and their applications

Micromechanical model	**Applications**	**Equations**
Benveniste-Miloh [12]	Composites with imperfect interfaces between constituents	Composites with prolate inclusions $\frac{\kappa_{e,33}}{\kappa_m} = 1 + V_f\left(1 + \frac{\kappa_f}{\kappa_m}B_1\right)h(\xi_0)$ $\frac{\kappa_{e,11}}{\kappa_m} = \frac{\kappa_{e,22}}{\kappa_m} = 1 + V_f\left(1 + \frac{\kappa_f}{\kappa_m}D_1\right)g(\xi_0)$ $\kappa_e = \frac{2}{3}\kappa_{e,11} + \frac{1}{3}\kappa_{e,33}$ B_1, D_1, ξ_0, h and g are defined in [10]. Composites with spherical inclusions

		$\frac{\kappa_e}{\kappa_m}$ $= \frac{2\kappa_m(1-V_f) + r\beta\left[1 + 2V_f + \frac{2\kappa_m}{\kappa_f}(1-V_f)\right]}{\kappa_m(2+V_f) + r\beta\left[1 - V_f + \frac{\kappa_m}{\kappa_f}(2+V_f)\right]}$ β is the interfacial conductance.
Hasselman-Johnson [13]	Composites with uniform distribution and low loading of spherical inclusions	$\frac{\kappa_e}{\kappa_m} = \frac{2V_f\left(\frac{\kappa_f}{\kappa_m} - \frac{\kappa_f}{rh} - 1\right) + \frac{\kappa_f}{\kappa_m} + \frac{2\kappa_f}{rh} + 2}{V_f\left(1 - \frac{\kappa_f}{\kappa_m} + \frac{\kappa_f}{rh}\right) + \frac{\kappa_f}{\kappa_m} + \frac{2\kappa_f}{rh} + 2}$ r is the radius of the sphere and h is the interfacial conductance.

5.1.2.2 Effective Medium Approach

In the effective medium approach (EMA), thermal conductivity is methodologically similar to electrical conductivity in terms of physical transport property. Therefore, the effective thermal resistance of PNCs can be estimated analogously to electrical resistance in which series and parallel arrangement can be derived, as shown in Figure 5.1. Theoretical assumptions in the derivation of the series and parallel models involve: (i) perfect interface between two phases in contact and (ii) independent contribution of the phases to the overall thermal resistance and conductance.

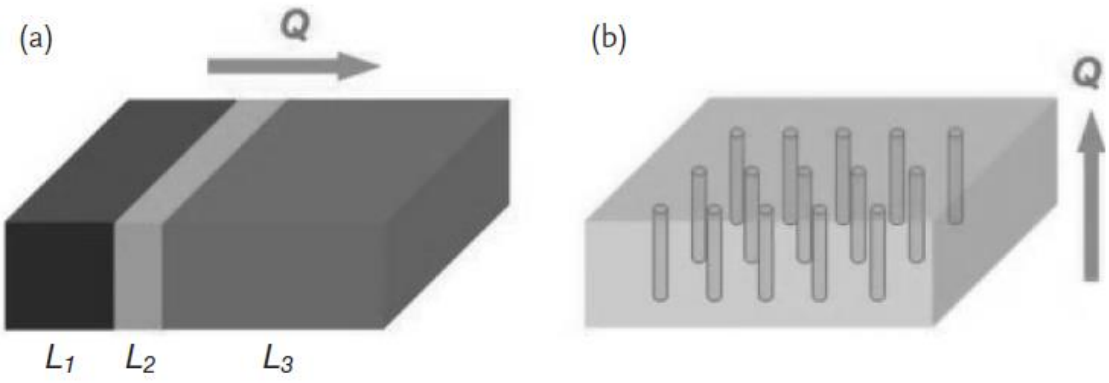

Figure 5.1: (a) Series and (b) parallel models [8].

In the case of series model, thermal resistance, R, is considered additive since the temperature drop along the heat flux direction is additive, that is [8]:

$$\frac{1}{\kappa_e} = \frac{1}{L}\sum_i R_i = \sum_i \frac{V_{f_i}}{\kappa_i} \ , \tag{5.28}$$

where $R_i = \frac{L_i}{\kappa_i}$ and $V_{f_i} = \frac{L_i}{L}$, κ_e is the overall thermal conductivity and L is the distance that the heat flux flows along. V_{f_i} is the volume fraction of nanofiller i. In case of parallel model, the effective thermal conductivity takes the form of Equation (5.29) [8].

$$\kappa_e = \sum_i V_{f_i}\kappa_i \ . \tag{5.29}$$

Although the series model is suitable for laminated composites along the stacking direction, it underestimates the thermal conductivity of particulate composites as it ignores interaction between the fillers. On the other hand, the parallel model applies readily well to continuous-filled composites along the fibre direction but overestimates the prediction of thermal conductivity of other types of composites. Consequently, the series and parallel models represent, respectively, the lower bound and upper bound for effective thermal conductivity of polymer-based composites. For PNCs, a more realistic prediction of thermal conductivity should account for randomness of particulate inclusions, interfacial thermal resistance of the matrix-particle blend, nanocomposites with multiphase components, and inclusion shape effect. For this purpose, a summary of improved thermal conductivity models for PNCs within EMA framework is provided in Table 5.3.

Table 5.3: EMA analytical models and their applications

EMA Model	**Applications**	**Expression**
Russel [14]	Composites with discrete pores dispersed in the matrix.	$\frac{\kappa_e}{\kappa_m} = \frac{V_f^{2/3} + \frac{\kappa_m}{\kappa_f}\left(1 - V_f^{2/3}\right)}{V_f^{2/3} - V_f + \frac{\kappa_m}{\kappa_f}\left(1 + V_f - V_f^{2/3}\right)}$ κ_m is the thermal conductivity of continuous matrix phase.
Tsao [15]	Composites with particulate inclusions.	$\frac{1}{\kappa_e} = \int_0^1 \frac{\mathrm{d}f_1}{\kappa_m + (\kappa_f - \kappa_m)\int_{f_1}^1 \frac{1}{\sigma\sqrt{2\pi}} e^{-0.5\left(\frac{f_1-\mu}{\sigma}\right)^2} \mathrm{d}f_1}$ f_1 is the one-dimensional porosity, μ is the mean of f_1 and σ is the standard deviation.

Cheng and Vachon [16]	Composites with particulate inclusions.	For $\kappa_f > \kappa_m$ $\frac{1}{\kappa_e} = \frac{1}{\sqrt{C(\kappa_f-\kappa_m)[\kappa_m+B(\kappa_f-\kappa_m)]}} \ln \frac{\sqrt{\kappa_m+B(\kappa_f-\kappa_m)}+\frac{B}{2}C(\kappa_f-\kappa_m)}{\sqrt{\kappa_m+B(\kappa_f-\kappa_m)}-\frac{B}{2}C(\kappa_f-\kappa_m)} + \frac{1-B}{\kappa_m}$ For $\kappa_f < \kappa_m$ $\frac{1}{\kappa_e} = \frac{2}{\sqrt{-C(\kappa_f-\kappa_m)[\kappa_m+B(\kappa_f-\kappa_m)]}} \tan^{-1} \sqrt{\frac{-C(\kappa_f-\kappa_m)}{\kappa_m+B(\kappa_f-\kappa_m)}} + \frac{1-B}{\kappa_m}$ $B = (3V_f/2)^{1/2}, C = -4/B.$
Maxwell [17]	Composites with: (i) spherical inclusions, (ii) very low filler loading (f), (iii), good dispersion, and (iv) no interfacial thermal resistance.	$\frac{\kappa_e}{\kappa_m} = 1 + 3V_f \frac{\kappa_f - \kappa_m}{2\kappa_m + \kappa_f - f(\kappa_f - \kappa_m)}$
Fricke [18]	Composites with: (i) arbitrarily shaped inclusions, (ii) very low filler loading (f), (iii) good dispersion, and (iv) no interfacial thermal resistance.	$\kappa_e = \kappa_m + \frac{2V_f}{3(1-V_f)} \sum_i^{a,b,c} \frac{\kappa_f - \kappa}{2 - abcL_i\left(1 - \frac{\kappa_f}{\kappa_m}\right)}$ where $L_i = \int_0^\infty \frac{\mathrm{d}t}{(i^2+t)\sqrt{(a^2+t)(b^2+t)(c^2+t)}}$ a, b and c are the three major axes of an ellipsoidal inclusion.
Hamilton-Crosser [19]	Multiphase composites.	$\frac{\kappa_e}{\kappa_m} = \frac{1 + \sum_{i=2}^m \frac{V_{f_i} i (n_i - 1)(\kappa_i - \kappa_m)}{\kappa_i + (n_i - 1)\kappa_m}}{1 - \sum_{i=2}^m \frac{V_{f_i} i (\kappa_i - \kappa_m)}{\kappa_i + (n_i - 1)\kappa_m}}$ where $n = 3/\Psi$, Ψ being the sphericity defined as the ratio of the surface area of a sphere to the surface area of the particle. m represents the number of phases in the composite.

Hashin-Lin-Wong [8, 20]	Particulate composites.	$2\left[2+c'+\frac{\kappa_f}{\kappa_m}(1-c')\right]\left(\frac{\kappa_e}{\kappa_m}\right)^2 - \left[2(1+2c')+\frac{\kappa_f}{\kappa_m}(1-4c') + 9\left(\frac{\kappa_f}{\kappa_m}-1\right)f\right]\frac{\kappa_e}{\kappa_m} - \left[2(1-c')+\frac{\kappa_f}{\kappa_m}(1+2c')\right] = 0$ where $c' = \frac{a^3}{(a+l_k)^3}$, $l_k = R_k\kappa_m$, R_k being the interfacial resistance.

5.2 Numerical Methods

Due to significant scale difference between the components of nanocomposites, direct use of micromechanical analytical models may lead to loss of accuracy in the predictions. Numerical method provides accurate predictions of the properties of PNCs based on realistic physical assumptions of the system. Practically, the choice of numerical method to investigate thermodynamics and kinetic properties, mechanical properties and interfacial molecular structure of nanocomposites depends on the length and time scales of interest. For this reason, numerical modelling of PNCs will be discussed under three headings, namely: Molecular, microscale and mesoscale/macroscale (continuum) approaches.

5.2.1 Molecular Scale Methods

Molecular scale methods (Figure 5.2) deal with interactions of atoms, molecules, or their clusters as basic units. The most popular techniques in this framework include molecular dynamics (MD), Monte Carlo (MC) and molecular mechanics (MM). In general, predicting the behaviour of PNC at this scale relies on thermodynamics and kinetics of the formation, molecular structure, and interactions.

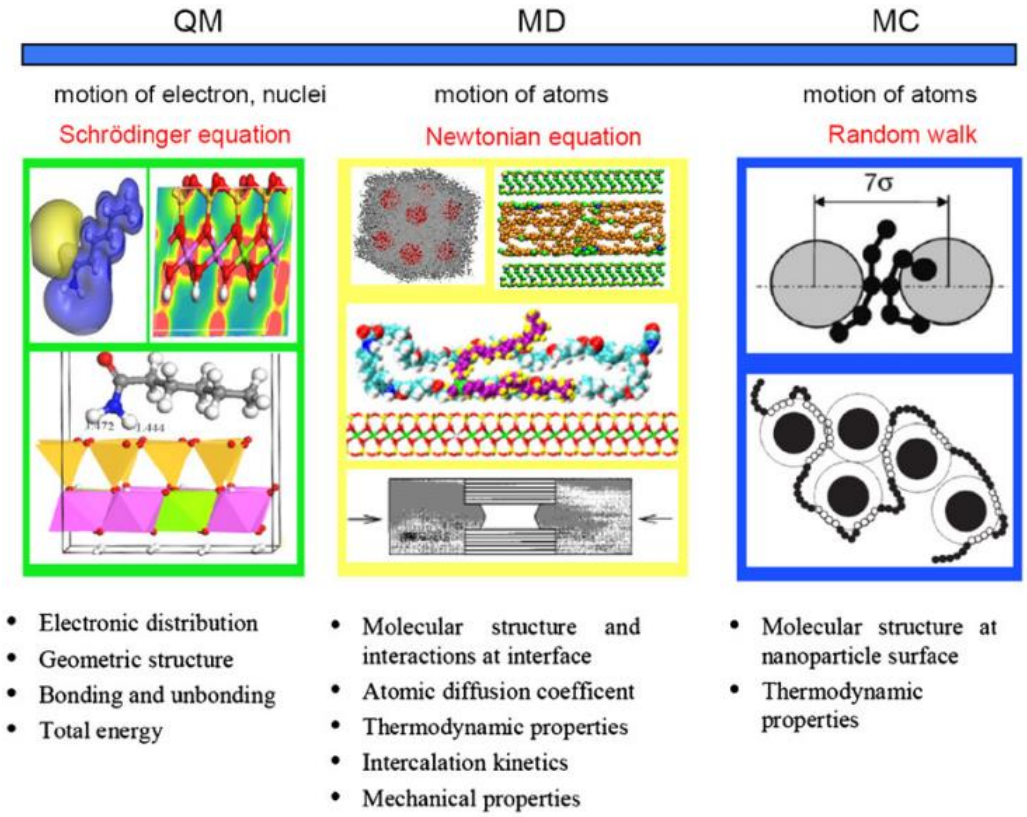

Figure 5.2: Molecular scale methods [2].

5.2.1.1 Molecular Dynamics

Molecular dynamics (MD) is suitable to investigate the effect of fillers on polymer structures and the effect of polymer-filler interactions on the materials properties of polymer composites. In this context, MD is used to predict the physical properties and time evolution of system of interacting particles, such as atoms and molecules [21,22]. Such information as atomic positions, velocities and forces are easily generated by MD, leading to derivation of macroscopic properties, such as heat capacities, pressure, and energy. Classical MD simulation is realised based on three components. Firstly, the initial positions and velocities of particles in a volume are defined. Secondly, the intermolecular or interatomic potential energy functions are defined. Finally, the evolution of the system in time is determined by solving Newton's equation of motion, given by Equation (5.30) [23].

$$\sum_i^n \vec{F}_{ij} = m_j \frac{\mathrm{d}\vec{r}_j}{\mathrm{d}t^2}, \tag{5.30}$$

where $\vec{F}_{ij}$ is the force exerted on the jth particle by the ith neighbouring particle at time t, while m_j and $\vec{r}_j$ are the mass and position of jth particle respectively, and n is the number of neighbouring particles. To complete an MD simulation, proper consideration must be given to

the choice of interatomic potentials, periodic boundary conditions, numerical integration scheme as well as pressure and temperature control to idealise meaningful thermodynamic set up [2]. The interactive forces between particles are calculated from interatomic potential energy function, which depends on the particle position, $\vec{r}$. Examples of methods that are used to determine the interactive force field include quantum method, empirical or quantum-empirical method. Typically, for an isolated system with n particles, the total energy, E can be expressed as the Hamiltonian Equation (5.31) [23].

$$\mathrm{E} = H = \sum_i^n \frac{\vec{p}_i^2}{2m_i} + U. \tag{5.31}$$

The first term in Equation (5.31) is the kinetic energy of the particles, where $\vec{p}_i$ represents the momentum of particle, i, whereas U is the potential energy, due to interatomic interactions. The interatomic potential, U depends on the nature of bonding among atoms. In this regard, different functions have been developed to characterise these bonds. Common examples of potential energy functions include:

- *Lennard-Jones Potential* [23]:

$$U(r) = \kappa\varepsilon\left[\left(\frac{\sigma}{r}\right)^n - \left(\frac{\sigma}{r}\right)^m\right], \tag{5.32}$$

where $\kappa = \frac{n}{n-m}\left(\frac{n}{m}\right)^{\frac{m}{n-m}}$, ε and σ are positive constants, while m and n are positive integers.

- *Moorse Potential* [23]:

$$U(r) = \Phi(r) = D\left[e^{-2\alpha(r-r_0)} - 2e^{-\alpha(r-r_0)}\right], \tag{5.33}$$

where D and α are constants and $r_0$is the equilibrium distance between two atoms.

- *Embedded Atom Potential* [23]

$$U_{\mathrm{tot}} = \sum_i E_e(\rho_i) + \frac{1}{2}\sum_{i,j(i\neq j)} \phi_{ij}(r), \tag{5.34}$$

in which ρ_i is the electron density of atom i, E_e is the embedding function, and ϕ_{ij} is the pair potential between particles i and j.

The force is related to the energy function through Equation (5.35) [23].

$$\vec{F}_j = m_j a_j = -\frac{\mathrm{dE}}{\mathrm{d}r_j} = -\frac{\mathrm{d}U}{\mathrm{d}r_j}. \tag{5.35}$$

in which $a_j = \frac{\mathrm{d}\vec{r}_j}{\mathrm{d}t^2}$.

In a case where molecular interaction is involved, a pair potential is not sufficient to capture the particle interaction, since molecules are characterised by covalent bonds [2]. In this case, apart from energy change due to change of bond length (E_{bond}), force field contributions arising from energy changes associated with a change in the bond angle (E_{angle}), molecular rotations ($E_{torsion}$), out-of-plane interactions between molecules (E_{oop}), other types of interaction energies ($E_{nonbond}$) or cross terms between other interaction terms (E_{cross}) may be significant. Therefore, the total energy of a molecule is expressed as Equation (5.36) [2].

$$\mathrm{E} = \mathrm{E_{bond}} + \mathrm{E_{angle}} + \mathrm{E_{torsion}} + \mathrm{E_{oop}} + \mathrm{E_{nonbond}} + \mathrm{E_{cross}} \quad (5.36)$$

In relation to Equation (5.35), the velocities are calculated from the accelerations while the positions are calculated from the velocities, using:

$$a_j = \frac{\mathrm{d}v_j}{\mathrm{d}t} \quad (5.37)$$

$$v_j = \frac{\mathrm{d}r_j}{\mathrm{d}t} \quad (5.38)$$

5.2.1.1.1 Time Integration

In MD simulations, the motion of a particle is evaluated over a large number of time-steps. Therefore, a robust integration scheme which minimises accumulated error during the simulation is required to solve the system of differential equations. Examples of techniques commonly employed include Verlet algorithm, Leap-frog algorithm, Velocity verlet, Beeman's algorithm, Symplectic reversible integrators and Gear predictor-corrector method [23, 24]. The general criteria for choosing an algorithm include [24]:

- *Computational efficiency*.
- *Accuracy for long time step integration*.
- *Conservation of energy and momentum*.
- *Time-reversibility, that is, the system should go back to the original state, when* $\delta t \rightarrow -\delta t$.

The Gear method [23] is explained here, due to its versatility. The Gear method uses prediction, evaluation, and correction steps to determine the particle position.

- *Prediction Step*

The particle position and its derivatives at time, $t + \Delta t$ are predicted using a truncated Taylor series in reference to the values of the position and its derivatives at time, t. The predicted position and its time-derivative are mathematically expressed as Equations (5.39)-(5.42) [23]:

$$r_j^p(t + \Delta t) = r_j(t) + \dot{r}_j(t)\Delta t + \ddot{r}_j(t)\frac{(\Delta t)^2}{2!} + \dddot{r}_j(t)\frac{(\Delta t)^3}{3!} \quad (5.39)$$

$$\dot{r}_j^p(t + \Delta t) = \dot{r}_j(t) + \ddot{r}_j(t)\Delta t + \dddot{r}_j(t)\frac{(\Delta t)^2}{2!} \quad (5.40)$$

$$\ddot{r}_j^p(t + \Delta t) = \ddot{r}_j(t) + \dddot{r}_j(t)\Delta t \quad (5.41)$$

$$\dddot{r}_j^p(t + \Delta t) = \dddot{r}_j(t) \quad (5.42)$$

The superimposed dot in Equations (5.39)-(5.42) represents temporal derivatives of the position of the corresponding order, while the superscript, p stands for the predicted value.

- *Evaluation Step*

The interatomic force at time, $t + \Delta t$ is calculated, using the predicted value of the position, r_j^p [23]:

$$\vec{F}_j = m_j a_j = -\frac{\mathrm{d}U\left(r_j^p\right)}{\mathrm{d}r_j^p} \quad (5.43)$$

- *Correction Step*

The discrepancy between the predicted value of the acceleration, $\ddot{r}_j^p$ and the evaluated value according to Equation (5.43), $\Delta\ddot{r}_j$, is used to correct the predicted values of the position and its derivatives, as shown in Equation (5.44) [23].

$$\Delta\ddot{r}_j = \left[\ddot{r}_j(t + \Delta t) - \ddot{r}_j^p(t + \Delta t)\right] \quad (5.44)$$

where $\ddot{r}_j(t + \Delta t)$ is the acceleration obtained from Equation (5.43). The corrected position and its derivatives are then expressed as follows [23]:

$$r_j^c(t + \Delta t) = r_j^p(t + \Delta t) + \frac{3}{32}\Delta\ddot{r}_j(\Delta t)^2 \quad (5.45)$$

$$\dot{r}_j^c(t+\Delta t) = \dot{r}_j^p(t+\Delta t) + \frac{251}{720}\Delta\ddot{r}_j(\Delta t)^2 \quad (5.46)$$

$$\ddot{r}_j^c(t+\Delta t) = \ddot{r}_j^p(t+\Delta t) + \Delta\ddot{r}_j \quad (5.47)$$

$$\dddot{r}_j^c(t+\Delta t) = \dddot{r}_j^p(t+\Delta t) + \frac{11}{6}\frac{\Delta\ddot{r}_j}{\Delta t} \quad (5.48)$$

Temperature and pressure control scheme is required in MD simulation, therefore appropriate thermostat algorithm is typically included to re-scale the velocities of the particles such that unrealistic fluctuations of the kinetic energy are suppressed. The Berendsen thermostat [24] is a popular scheme that roughly yields correct canonical ensemble for large systems.

5.2.1.2 Monte Carlo

Monte Carlo (MC) is a stochastic method, which relies on random sampling to compute the properties of a system. In the context of PNCs, MC techniques are suitable to investigate molecular response of nanoparticles under the influence of various factors. These factors include, but are not limited to, number of variables bounded to different constraints, accuracy of input parameters and constraints [2]. Unlike deterministic models including MD, MC models take into account risks associated with variation of input parameters. Typically, a statistical distribution is used as the source for each of the input parameters, followed by drawing random samples from each distribution to serve as the input variables. Then, output parameters corresponding to different input parameters are collected from a number of runs for statistical analysis and decision making. Summarily, to model a physical process, MC technique uses four steps [25]:

- *Static model generation* – a deterministic model characterising the real scenario is developed, using the most likely value of the input parameters.
- *Input distribution identification* – the deterministic model is translated into analogous statistical model based on stochastic nature of the input variables. Precisely, historical data of the input variables is used to identify the underlying distributions.
- *Random variable generation* – in this step, the statistical model generated from different input distributions is solved by numerical stochastic sampling experiment.
- *Analysis and decision making* – the sample of output variables collected from the simulation is statistically analysed to provide information for decision making.

Considering a canonical (NVT)[a] ensemble with N atoms at temperature T, a new configuration for an atom is formed by arbitrarily translating the atom position from point i to j, in which the change in Hamiltonian, H is computed as Equation (5.49) [2].

$$\Delta H = H_j - H_i \tag{5.49}$$

where H_i and H_j are Hamiltonian corresponding to positions i and j, respectively. The new atomic configuration is accepted, depending on the direction of ΔH, which reduces the energy of the system. Typically, the new configuration is accepted if:

$$\begin{cases} \Delta H < 0 \\ \Delta H \geq 0 \quad \text{subject to probability } p \end{cases} \tag{5.50}$$

in which p is given by Equation (5.51) [2].

$$p \propto \exp\left(-\frac{\Delta H}{k_B T}\right) \tag{5.51}$$

where k_B is the Boltzmann constant and T is the absolute temperature of the particle.

According to [1], the new configuration may be accepted subject to:

$$\varsigma \leq \exp\left(-\frac{\Delta H}{k_B T}\right) \tag{5.52}$$

where ς is a random number between 0 and 1, that is, $0 < \varsigma < 1$. In case Equation (5.52) is not satisfied, the new configuration is rejected, and the original position is retained. The process is then repeated for other arbitrarily selected atoms until equilibrium is attained.

Note[a]: NVT ensemble is a system whose internal states are controlled by thermodynamic variable (for example, absolute temperature, T) and mechanical variables (for example, number of particles, N and volume of system, V).

5.2.2 Microscale Methods

Microscale techniques are aimed at combining the merits of molecular scale and macroscale (continuum) methods, while avoiding their disadvantages. Therefore, microscale method is suitable to study the microscopic structure and phase separation of PNCs. In these methods, the polymer is characterised with a field representing microscopic particles in which molecular details are implicitly embedded. This approach is computationally beneficial given that the

behaviour of nanoparticles can be simulated on length and time scales, which is inaccessible by molecular scale methods.

5.2.2.1 Lattice Boltzmann Method

Lattice Boltzmann (LB) method is popular for efficient simulation of fluid flow, and it has been adopted for investigating phase separation of binary fluids in the presence of solid particles. One of the major advantages of LB method is the convenience to incorporate microscopic physical interactions of the fluid particles into the numerical model [2]. Therefore, it is possible to couple LB method with molecular scale method, such as MD. The main disadvantage of LB method is the numerical instability of the simulation, which may be associated with high interparticle interaction strength or high forcing rate.

LB technique involves a collection of fictitious particles, residing on the nodes of regular shape lattices, interacting according to simple rules. To describe a particle occupation in LB method, a distribution function of particle velocity along i direction, $n_i(x,t)(i = 1, \dots, N)$ is defined, where N denotes the number of directions of the particle velocities at each node, and the evolution rule for updating lattice site occupation by the particles in a given time step is defined based on the discrete velocity model for a multicomponent ($c = 1, \dots, M$) flow [24]:

$$f_i^c(x + e_i\delta_x, t + \delta_t) = f_i^c(x,t) + \Omega_i\left(f_i^c(x,t)\right) \qquad i = 1, \dots, N, \tag{5.53}$$

where t is the time, e_i is the discrete velocity vector in i direction, and Ω_i is the collision operator in i direction representing changes, due to pairwise collisions. In LB method, at each time step, particles at each lattice points move to the nearest nodal points in the lattice in accordance with the direction of velocity (a process called streaming). Then, interaction of particles occurs, leading to change in the velocity directions of the particles (a process called collision or redistribution). A typical lattice structure is defined by the problem dimension, d and the number of lattice vectors, n_v and is compactly represented as $\mathrm{DdQ}n_v$. For example, Figure 5.3 depicts the discretised 2D with nine velocity vectors.

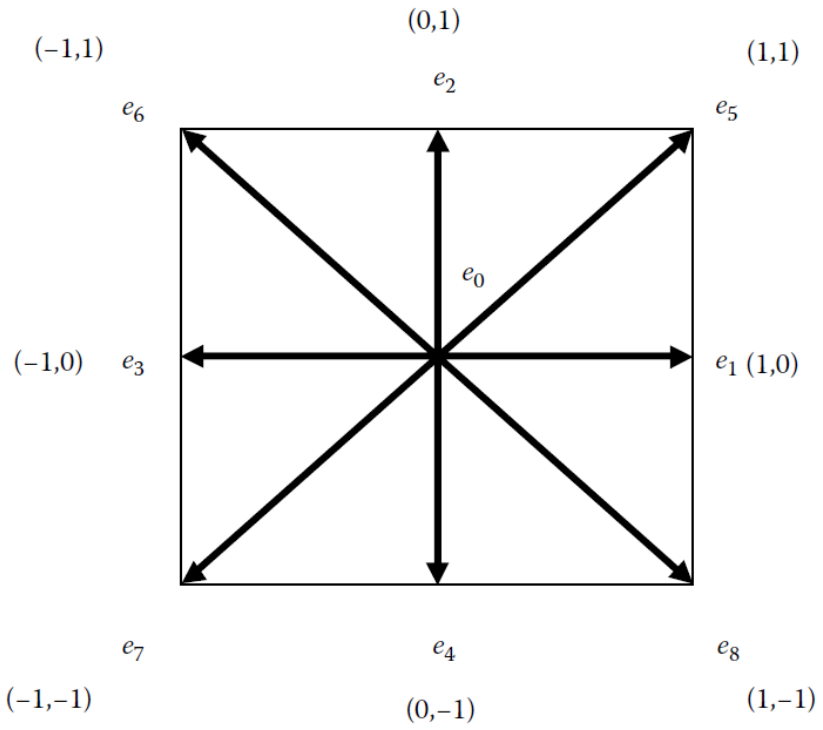

Figure 5.3: Nine velocity vectors of D2Q9 lattice [23].

To characterise the pairwise collision, the collision operator can be expressed in different ways. For example, a simple operator in the form of linear Bhatnagar-Gross-Krook, which uses single relaxation time is expressed as Equation (5.54) [24].

$$\Omega_i = -\frac{1}{\tau^c}\left(f_i^c - f_i^{c,eq}\right) \tag{5.54}$$

where $f_i^{c,eq}$ corresponds to local equilibrium distribution function of f_i^c and τ^c is the viscosity-related dimensionless collision relaxation time of component c of the fluid (polymer). The relaxation parameter is related to the fluid kinematic viscosity of fluid component c, v^c, through Equation (5.55) [24].

$$\tau^c = \frac{v^c}{s^2} + \frac{1}{2} \tag{5.55}$$

where $s = 1/\sqrt{3}$ is the lattice speed for unit spacing lattice structure.

In some applications, where stability issues are encountered due to fixed Prandtl number associated with single-relaxation collision operator, the multiple-relaxation collision operator is preferred. Multiple-relaxation collision technique is suitable for varying kinematic and bulk viscosities and incorporates mechanisms for improved stability of the simulation.

5.2.2.2 Brownian Dynamics

Brownian dynamics (BD) technique allows simulation of particles on the microsecond timescale, whereas MD technique permits particle simulation up to a few nanoseconds. Unlike in MD where there is explicit description of solvent molecules, in BD an implicit description of solvent particles is applied in a continuum sense while ignoring internal motions of the molecules. The objective of the BD technique is achieved by accounting for the effect of solvent molecules on the polymer through dissipative and random force terms so that the governing equation of motion becomes Equation (5.56) [2].

$$F_i(t) = \sum_{i \neq j}^{n} F_{ij} - \alpha\mu_i + \beta\tau_i(t), \qquad (5.56)$$

Equation (5.56) is the Langevin equation, where F_{ij} is the force applied by particle, j on particle i, α and β are system-dependent constants, μ_i is the momentum of particle, i, and τ_i is a Gaussian random noise term. The approximation in Equation (5.56) leads to fluctuating forces such that energy and momentum are no longer conserved. Since Equation (5.56) does not obey the Navier-Stokes equations, BD method is only suitable to simulate the diffusion properties but cannot reproduce the hydrodynamic flow properties of the system.

5.2.2.3 Dissipative Particle Dynamics

Dissipative particle dynamics (DPD) is a particle-based method, such as MD and BD techniques and is suitable for both Newtonian and non-Newtonian fluids on microscopic length and time scales. The basic unit of DPD is a molecular assembly (representing a particle) which is characterised by its mass, m_i, position, r_i and momentum, μ_i. The force describing the interactions between two DPD particles may be expressed as a sum of the conservative, F_{ij}^C, dissipative, F_{ij}^D and random, F_{ij}^R forces given in Equation (5.58) as [2]:

$$F_{ij} = F_{ij}^C + F_{ij}^D + F_{ij}^R, \qquad (5.57)$$

The total force, F_i acting on a particle, i at time, t is given in Equation (5.58) [2].

$$F_i = \sum_{j \neq i} F_{ij}^C + F_{ij}^D + F_{ij}^R, \qquad (5.58)$$

According to Equation (5.58), the macroscopic behaviour of DPD particles incorporates Navier-Stokes hydrodynamics, due to conservation of momentum. In comparison with MD, larger time steps are allowed in DPD simulation and hydrodynamic equilibrium is attained in DPD system with far fewer particles.

5.2.3 Mesoscale and Macroscopic Methods

Notwithstanding the importance of molecular scale and microscale modelling, molecular properties of PNCs can be homogenised macroscopically according to different scales. As a result, in the macroscopic scale, the discrete atomic and molecular structure is ignored while continuity of material distributed throughout the control volume is adopted. The basis of macroscopic scale methods lies in the compliance with fundamental laws of continuity, equilibrium, momentum, conservation of energy and conservation of entropy [2]. By employing appropriate constitutive relations and equation of state, the macroscale method measures the deformation of a continuum as a result of external forces by the resulting internal stresses and strains.

5.2.3.1 Micromechanics Approach

Micromechanics approach relies on the development of RVE to characterise local continuum properties, since the uniformity of continuum may not hold at the macroscopic scale (Figure 5.4). The RVE is periodically arranged in consistent with the smallest constituent that significantly affects the macroscopic behaviour. Therefore, micromechanics approach can assess discontinuities and interfacial profile of different constituents in a continuum. In addition, micromechanics approach allows for coupling between mechanical and non-mechanical properties. In the context of PNCs, micromechanics methods tend to satisfy the following basic assumptions [2]:

- *Linear elasticity of fillers and polymer matrix*: This assumption suggests that a linear relationship exists between the total stress, $\boldsymbol{\sigma}$ and the infinitesimal strain tensors, $\boldsymbol{\varepsilon}$ for the matrix and nanophase constituents, using:

$$\boldsymbol{\sigma}^f = \boldsymbol{C}^f \boldsymbol{\varepsilon}^f \tag{5.59}$$

$$\boldsymbol{\sigma}^m = \boldsymbol{C}^m \boldsymbol{\varepsilon}^m \tag{5.60}$$

  where $\boldsymbol{C}^m$ and $\boldsymbol{C}^f$ are the stiffness tensors for the matrix and fillers, respectively.

- *Axisymmetric shape of fillers that are defined by aspect ratio*: Since the local stress and strains are non-uniform throughout the PNC continuum, volume average stress and strain resultants are defined over the representative averaging volume, V, as:

$$\overline{\boldsymbol{\sigma}} = \frac{1}{V}\int_V \boldsymbol{\sigma}(x)\mathrm{d}V \tag{5.61}$$

$$\bar{\boldsymbol{\varepsilon}} = \frac{1}{V}\int_V \boldsymbol{\varepsilon}(x)\mathrm{d}V \tag{5.62}$$

The equivalent average stress and strain tensors of the fillers and matrix are expressed as:

$$\bar{\boldsymbol{\sigma}}^c = \frac{1}{V^c}\int_{V^c} \boldsymbol{\sigma}(x)\mathrm{d}V \tag{5.63}$$

$$\bar{\boldsymbol{\varepsilon}}^c = \frac{1}{V^c}\int_{V^c} \boldsymbol{\varepsilon}(x)\mathrm{d}V \tag{5.64}$$

where c denotes the filler, f or polymer matrix, m component. On this basis, the total average stress and strain are related to the filler and matrix averages according to

$$\bar{\boldsymbol{\sigma}} = v^f\bar{\boldsymbol{\sigma}}^f + v^m\bar{\boldsymbol{\sigma}}^m \tag{5.65}$$

$$\bar{\boldsymbol{\varepsilon}} = v^f\bar{\boldsymbol{\varepsilon}}^f + v^m\bar{\boldsymbol{\varepsilon}}^m \tag{5.66}$$

- *Perfect bond between fillers and polymer matrix*: The average properties of composite stiffness, $\boldsymbol{C}$ relate the average stress to the average strain tensors according to

$$\bar{\boldsymbol{\sigma}} = \boldsymbol{C}\bar{\boldsymbol{\varepsilon}} \tag{5.67}$$

in which $\boldsymbol{C}$ is related to the filler and matrix stiffness tensors according to

$$\boldsymbol{C} = \boldsymbol{C}^m + v^f(\boldsymbol{C}^f - \boldsymbol{C}^m)\boldsymbol{A}.$$

where $\boldsymbol{A}$ is the strain concentration tensor, defined as the ratio between the average filler strain $\bar{\boldsymbol{\varepsilon}}^f$ and the average strain $\bar{\boldsymbol{\varepsilon}}$, is given as

$$\bar{\boldsymbol{\varepsilon}}^f = \boldsymbol{A}\bar{\boldsymbol{\varepsilon}} \tag{5.68}$$

5.2.3.2 Equivalent-Continuum Approach

Classical micromechanics approach lacks the capacity to simulate the behaviours of nanotube-reinforced composites, due to significant scale difference. The equivalent-continuum (EC) approach, proposed in [26], is a multiscale approach, which incorporates molecular, microscopic and continuum scales to model nanotube-reinforced composites, such as single-walled carbon nanotube (SWCNT) composites.

In the first stage of EC simulation, the equilibrium structure of the polymer composite is generated with MD technique in which the potential energy of the SWCNT-polymer composite system is defined according to MD principles. Then, an equivalent-truss model is used to

construct the RVE, where each truss element represents an atomic interaction and each pin-joint of the truss corresponds to an atom in the molecular model (Figure 5.4).

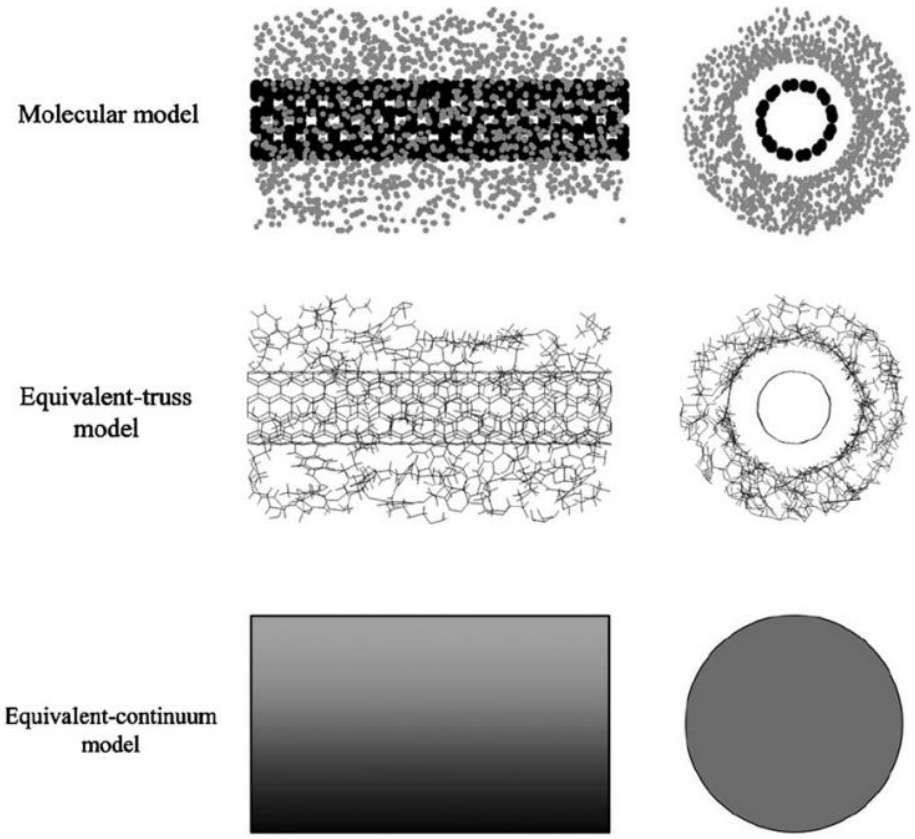

Figure 5.4: Representative volume elements of computational model at different length scale [2].

Therefore, the equivalent-truss model represents the intermediate link between MD and EC systems. By equating the potential energy of the effective fibre, U^f with the potential energies of MD and equivalent-truss models, U^{MD} and U^t, respectively, the relationship between the elastic stiffness tensor of the effective fibre and the force constants of the MD system can be established as Equation (5.69) [2].

$$U^f = U^{MD} = U^t \tag{5.69}$$

By applying a set of loading conditions to Equation (5.69), the components of the elastic stiffness tensor of the effective fibre can be determined. Then, based on the mechanical properties of the effective fibre and the bulk polymer, the general constitutive properties of the SWCNT-based PNC can be determined, using appropriate micromechanics model, such as MT and HT models [2].

5.2.3.3 Finite Element Method

Finite element method (FEM) is a numerical method developed to approximate solution of differential equations. FEM relies on the generation of mesh to idealise a structure and capture the response under complex loading, material, and geometric conditions. The procedure for the implementation of FEM starts with the replacement of the continuum with finite elements constituting subdomains of the continuum. Finite elements are defined by shape functions, which is used to transform the element topology and approximate state variables at the element nodes. Appropriate constitutive laws are then selected to define the relationship between strain and stress fields, followed by application of the variational principle to describe the strain energy of the problem over each finite element. The total elastic energy in the continuum model, neglecting traction and body forces, is given by the sum of potential and kinetic energies [2]:

$$U = U^p + U^k \tag{5.70}$$

where U^p denotes the potential energy expressed in the sample volume of the continuum and is given by Equation (5.71).

$$U^p = \frac{1}{2}\int \boldsymbol{\varepsilon}^{\mathrm{T}}\boldsymbol{C}\boldsymbol{\varepsilon}\mathrm{dV}, \tag{5.71}$$

in which $\boldsymbol{\varepsilon}$ represents the strain tensor, while $\boldsymbol{C}$ is the elastic stiffness tensor. The kinetic energy in the sample volume is denoted as U^k and is expressed as:

$$U^k = \int \rho \frac{\partial^2 \boldsymbol{u}}{\partial t^2}\mathrm{dV} \tag{5.72}$$

By replacing the continuum state variables in Equations (5.71) and (5.72) with discrete variables defined by set of shape functions, system of elemental equations is formed and subsequently assembled to form the global system of equations. The global system is numerically solved to determine the unknown state variables, which are consequently used to compute the stresses and strains of the PNC structure.

5.2.4 Multiscale Modelling

One of the main goals of simulation of PNCs is the accurate prediction of their hierarchical structures and properties. Towards enhancing the properties of PNCs for high-technology applications, structural characterisation, and precise manipulation of the fabrication of the nanostructured materials must be achieved. This implies that the nanocomposite structure as

well as physical and chemical processes at the nanoscale level significantly influence the final properties of PNCs. Therefore, an adaptable modelling strategy is required to explore the design of PNC materials for optimised performance.

Prediction of PNC behaviour based on application of analytical and numerical models at different independent scales is challenging considering length scales up to six orders of magnitudes or time scales spanning a dozen orders of magnitude (Figure 5.5), thus impeding the simulation efficiency [8]. Given this reality, it is impracticable for a single model to explore these length and time scales. Multiscale modelling is a practical way to bridge different length and time scales via combined computational methods that can simulate fundamental molecular processes and seamlessly transfer numerical parameters efficiently across wide scales to satisfactorily predict macroscale properties. In this context, two multiscale approaches that span from molecular to macroscopic levels are known as sequential and concurrent methods, as subsequently elucidated:

- *Sequential Multiscale Method*: This involves linking of hierarchical computational methods in a manner that allows the computation of operative parameters of a model on large scale from the calculated quantities obtained at a lower scale of the model [2]. Example of simulation tools designed to perform sequential multiscale modelling is OCTA developed by Doi [27]. OCTA relies on multiple simulation engines to facilitate modelling of polymers from molecular scale up to the mesoscale.
- *Concurrent Approach*: This uses a combination of several computational methods linked together to bridge different scales of material behaviour concurrently [2]. Although this approach is computationally promising, considering the potential for seamless interaction between different scales of material behaviour, the method is in its early stage of development and thus, it has a limited application.

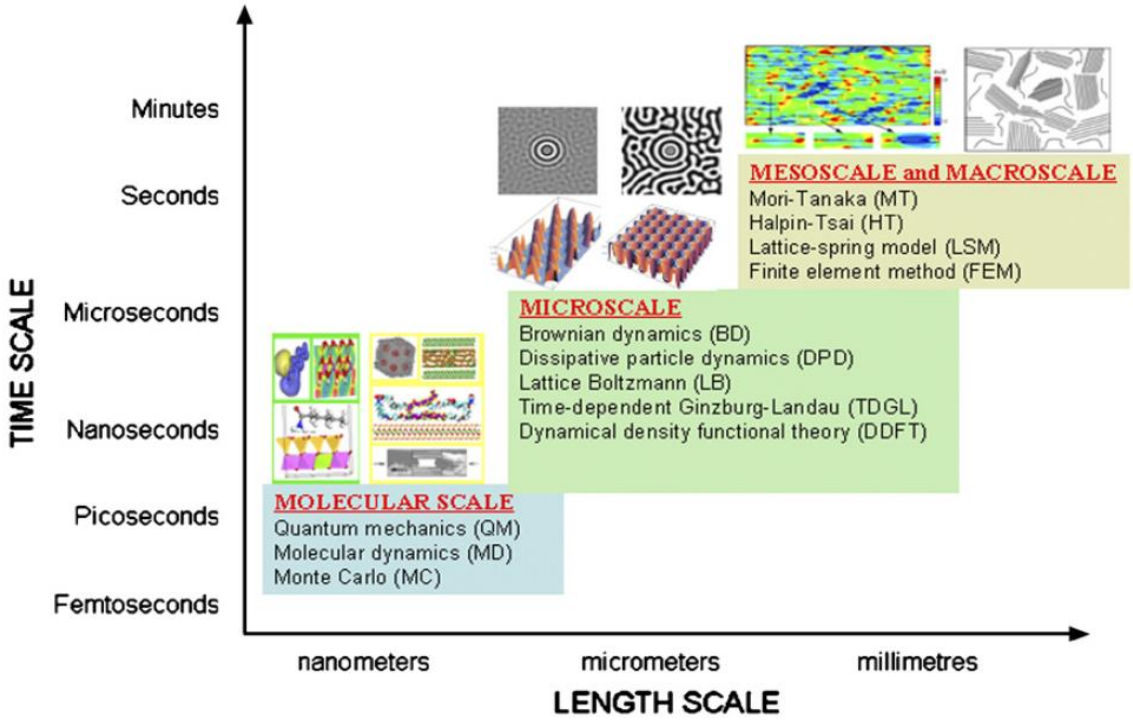

Figure 5.5: Hierarchical settings of PNC structure in time and length dimensions [2].

Over the years, varieties of computational methods have been developed to efficiently capture phenomena at each length and time scale. For example, Quantum mechanics methods are available to simulate systems containing atoms, while MD or MC methods are suitable for capturing material properties at atomic level. At the mesoscale level, BD or DPD approaches are examples of methods relevant to investigate mesoscale properties of polymer-based materials, while FEM possesses excellent potential to capture macroscopic properties of the system. The goal of multiscale modelling is to exploit the individual capacities of these methods, beginning from the quantum scale all the way to the process scale to predict the macroscopic properties of an engineering system of interest. Fundamentally, the key ingredients to construct a successful multiscale modelling are: (i) information about the basic processes that control the system at the lower scales and (ii) reliable strategies to link the degrees of freedom from the lower scale to the coarser scale [8].

In the context of polymer-based nanocomposites, the coarsening process at the lower scale, for example from QM to MD, is based on fundamental principles and can be generalised. However, the larger range of length and time scales that define the macromolecules constitutes specific challenges that complicate coarsening process at higher scales. As a result, scale integration in the specific context of PNCs can be achieved in different ways. At the lower scale, scale

integration is based on force field application that retrieves information from the quantum chemistry to the atomistic model. At the mesoscale level, essential features of the atomistic systems must be preserved structurally or thermodynamically, or both [28]. Finally, the most challenging aspect toward practical design application of material is linking to the mesoscale in which the microstructural features of PNCs are described to predict the property at the macroscopic level.

As an example of hierarchical multiscale computational process, montmorillonite (MMT)/poly (ethylene oxide) (PEO) - based PNC was investigated [29] to determine the effect of PEO molecular weight and the presence of water molecules on the interactions between polymer and clay platelets. Firstly, atomistic MD simulation of PEO-based PNC was carried out in a solvated environment to retrieve energetical (binding energy) and structural (interaction energy and chain conformation) information at the molecular level [30]. Then, the mesoscale property prediction was achieved by adopting the DPD approach in which the data gathered at the atomistic scale were projected to the corresponding energetical and structural information required to set up a coarse-grained mesoscale simulation. The mesoscale simulation produced information on the morphologies and density distribution of the system, which served as basic inputs to finite element simulation that was used to predict the property of the system at the macroscale level.

5.2.4.1 Stochastic Multiscale Approach

The random dispersion of reinforcing phases in PNCs significantly affects the microstructural properties which in turn influence the macroscopic behaviours. Other issues affecting the microstructural behaviours of PNCs include the size, orientation, and shape of the nanophases. Given these challenges, there is limited control in the manufacturing of tailored PNC materials, leading to uncertainties in the actual mechanical properties of the PNC constituents. In the context of modelling, critical experimental information may be omitted in the assumptions and approximations used to develop the PNC model. Besides, in the case of mixing phases that span multiple structural length scale, the load transfer mechanisms between the polymer matrix and nanophases are multiscale in nature. Consequently, the mechanical properties of PNCs are uncertain and substantial disparities may occur between experimentally measured mechanical properties and predictions by analytical or numerical calculations [31, 32]. To incorporate the spatial randomness induced by the nonuniform distribution of constituent phases in polymers, multiscale stochastic finite element method (MSFEM) has been proposed [33]. In MSFEM, the

PNC is assumed to constitute a random heterogeneous media, due to random behaviours and uncertainties in the overall material behaviours. On this basis, a multiscale micromechanical approach is used to homogenise the system to obtain the estimates of local mechanical properties. This step is followed by Monte Carlo finite element scheme, which uses the local properties as inputs to compute the bulk properties of the PNC.

The procedure required to implement MSFEM can be summarised into four steps [33]:

- *Definition of material region*: A RVE that structurally captures the whole mixture on average and encapsulates sufficient number of inclusions is firstly defined. Other types of representative material regions include statistical volume element (SVE) [34] or statistically equivalent RVE (SERVE) [35], which incorporate separation of scale, have been proposed. According to [35], SERVE is suitable to compute local mechanical properties, as dictated by the actual randomness induced by the non-uniform dispersion of nanophase constituents in the PNC microstructure.
- *Identification of spatial randomness*: To capture heterogeneities, which induce randomness in the PNC structure, MSFEM statistically quantifies the variations of the volume fractions of nanophase constituents. The relative concentration of the nanophase constituents in the material region are assumed to be equivalent to the total amount of nanofillers in the PNC. According to Figure 5.6, variations observed in the volume fraction values of SWCNT are captured at the grid of material points in the material region through creation of a random field based on probability distribution functions [33].

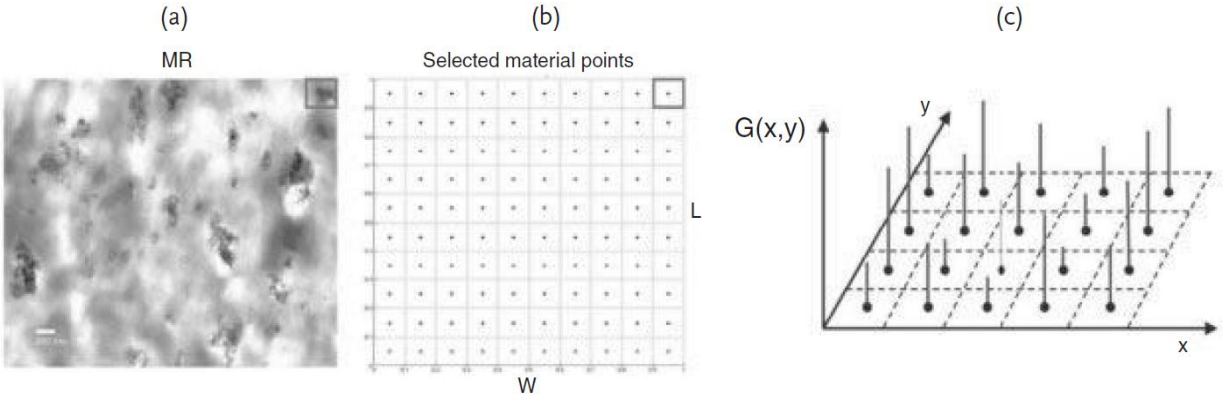

Figure 5.6: (a) Material region (MR), (b) material points with random CNT volume fraction (c) discretised random field for variation of SWCNT in polymers [33].

- *Homogenisation of multiscale properties*: MSFEM determines the local properties of the PNC at the sub-element level of the material region (Figure 5.7). In MSFEM, homogenisation process is performed in two stages based on MT method to determine the stiffness tensor of homogenised spherical inclusions (*IN*) and the modified matrix (*MM*) in each FE in the material region. A two-phase media, which comprises a modified matrix and spherical inclusions, is adopted [36] to determine the effect of SWCNT dispersion and agglomeration on the mechanical properties of CNT-based PNC.

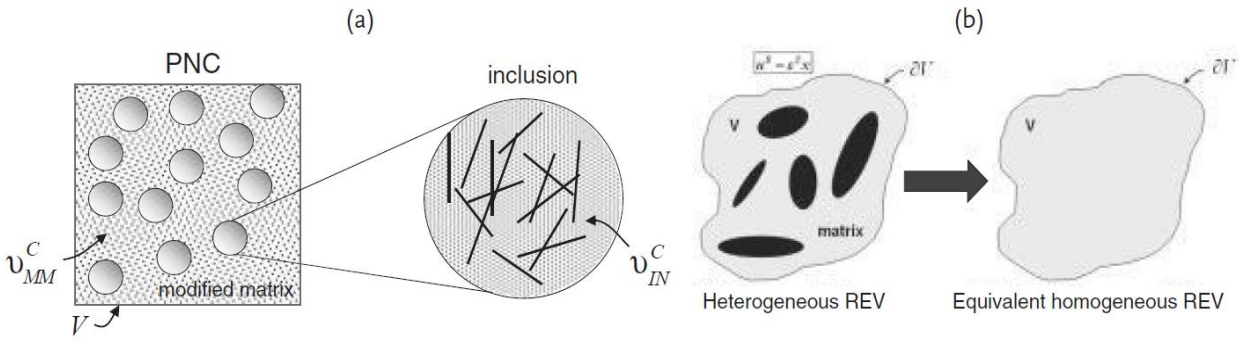

Figure 5.7: (a) Sub-element material structure in a finite element and (b) RVE homogenisation procedure [33].

- *Monte Carlo finite element model*: MSFEM determines the overall mechanical properties of the PNC system by numerically solving elasticity problem in line with conventional FE principles, except that the constitutive parameters are random values obtained according to Monte Carlo method.

5.3. Computational Approach to PNC Property Predictions

5.3.1 Stiffness and Strength

The analytical and numerical models describe above can be used to predict mechanical properties, such as strength and stiffness (elastic modulus), which are significantly influenced by the PNC filler size and polymer configuration [1]. In this context, extended micromechanical models have been adopted to predict the properties of PNCs [37,38]. For example, micromechanical-based MT model has been combined with the probability distribution function (PDF) of the Doi-Hess hydrodynamic theory to predict the effective elastic properties of stationary and flow-induced nanorod-based PNC [37]. Considering a

perfect bonding arrangement between inclusions and matrix, an effective stiffness tensor which is valid for any volume fraction was derived according to the MT theory. The symmetry regarding the orientational distributions of the effective stiffness tensor of nano-rod composites are inherited from probability distribution functions (PDFs). The volume fraction dependent effective moduli can be consequently determined by implementing the MT formula using numerical databases for the PDFs [37].

Micromechanical models have also been used to predict the mechanical properties of nanotube-based PNC containing complex inclusions, where the Eshelby's equivalent tensor is combined with MT type model having two aspect ratios to evaluate the longitudinal and shear moduli [38]. Given the constitutive equations for inclusion and matrix materials (see Equations 5.59-5.66), the volume-average stresses and strains were determined through integration of non-uniform local quantities over a large volume of the material filled with inclusions. The effective moduli of the PNC are eventually evaluated in terms of the average stresses and strains [38]. Moreover, to predict the interfacial strength of SWCNT-based PNC, a modified Kelly-Tyson approach (continuum-based method) has been proposed under the assumption of uniform interfacial shear and axial normal stresses [39]. The continuum mechanics approach, often combined with suitable micromechanical method, is another strategy to predict the mechanical properties of PNCs.

In the aspect of numerical methods, Mokashi et al. [40] proposed a procedure based on molecular mechanics approach to obtain the tensile properties (specifically both elastic modulus and strength) of PNC, in which the atomic structure of the polymer matrix is first generated in the simulation cell using computer algorithm, and relaxed to an equilibrium configuration whose parameters are recorded [40]. Then, the atomic structure of the nanofillers (for example, SWCNT) are generated and the coordinates merged with the polymer structure. Tensile boundary and loading conditions, similar to mechanical testing, are applied to the atoms at the boundaries of the simulation cell of the nanocomposite system. In each step of the incremental longitudinal displacement, the system is relaxed to an energetically stable state and this process is repeated until the polymer chains fracture. The tensile strength is determined from the total force, along the direction of the incremental displacement, acting on the boundary atoms per unit area of the cross-section.

A multiscale strategy comprising FEM approach and micromechanical method (for example, MT method) has been extensively explored to predict the elastic properties of wavy or

randomly oriented nanotube-based PNCs and silica nanoparticle-based PNC [41-43]. To investigate the effect of characteristic waviness of nanotubes embedded in polymers on the effective stiffness of nanotube-reinforced polymers, a 3D FEM model was used to numerically compute dilute strain concentration tensor. Thereafter, the concentration tensor was used to predict the effective modulus of the PNC with aligned or randomly oriented inclusions based on MT theory [42]. It is noted that for accurate prediction with this approach, especially in the case of high particle loading, it is important to account for the properties of the interface between matrix and the particles. In terms of accuracy of the FEM-micromechanical approach, fibre volume fraction is a significant factor to be considered when predicting stiffness properties of PNCs. For PNC with low fibre volume fraction, MT method can accurately predict the stiffness of PNC [44]. Above a critical volume fraction, FEM-based models possess superior accuracy over MT micromechanical models, especially when handling complex fibre-polymer interactions.

5.3.2 Stress Transfer

The mechanical properties of PNC with high disparity in the modulus of its constituents (polymer and nanoparticles) are strongly influenced by stress-transfer mechanism. This is the case for clay/polymer nanocomposites, where clay nanoparticles exhibit much higher modulus than the polymer matrices, and there is presence of large interfacial area between the thin nanoclay platelets and the polymer. Therefore, due to the dominant role of the interfacial properties, stress transfer mechanism between rigid nanoparticles and the polymer plays significant role in the modulus and strength properties [45].

Characterising the interfacial properties of PNCs is an effective way to determine the level of stress or load transfer (interfacial adhesion). This can be achieved using MD [46], molecular mechanics (MM) [47], continuum mechanics (CM) [48], or analytical approach [45]. Essentially, the interfacial shear stress is calculated based on the conditions of perfect or imperfect bonding, which determine the reinforcing efficiency of the fillers. Perfect bonding is a simple assumption that can lead to over-prediction of the mechanical properties, since the aspect ratio and volume fraction may be overestimated. Nonetheless, for certain PNCs, such as nanoclay-based types, complete adhesion can be achieved at low concentration of clay platelets and a perfect bonding assumption can be justified. Under imperfect bonding condition, which applies for many PNCs, there is incomplete stress transfer at the polymer-filler interface, necessitating the estimation of effective parameters for the calculation of mechanical

parameters. For example, to determine the modulus of PNC under imperfect bonding condition, the effective aspect ratio and effective volume fraction must be calculated to enhance the accuracy of the prediction [45].

MD simulation has proved effective for estimating the shear strength and critical length required to enhance the load transfer capacity of nanotube-based composite [46]. The model system comprises a SWCNT embedded into a crystalline or amorphous matrix and subjected to a periodic boundary condition. In addition, the intramolecular interactions in the nanotube, polymer chains and cross-links are characterised by many-body potential function which allows the formation of chemical bonds between the nanotube and polymer matrix. The non-bonded interactions are captured by Lennard-Jones potentials. The polymer-nanotube system was equilibrated using MD simulation to create zero initial stress state. In the next step, further MD simulation was carried out with a uniform one-body force added to the atoms that comprise the nanotubes to determine the minimum shear strength required to pull the nanotube through the polymer matrices (i.e., crystalline, and amorphous). The shear strength, τ_c, is estimated as the total force at which the centre mass of the nanotube began to move freely independent of the matrix. Finally, the critical length of nanotube that guarantees strong load transfer is estimated from τ_c as [46]:

$$l_c = \frac{\sigma_f \mathrm{d}_f}{\tau_c} \tag{5.73}$$

where σ_f represents the fibre tensile strength and d_f denotes the fibre diameter.

5.3.3 Fatigue and fracture

Studies have demonstrated that, without compromising the stiffness, nanoparticles have the ability to improve the fatigue resistance of polymer nanocomposites through crack-bridging and a frictional pull-out mechanism [1]. To determine the fatigue response of PNC, a good model should capture different mechanisms responsible for fatigue resistance, which include crack pinning, fibre bridging, crack tip deflection and particle debonding (fibre pull-out). The dominating mechanism depends on the nature of polymer-nanofiller mix. Fibre pull-out is the main mechanism of fatigue failure in CNT-based nanocomposites. A fracture mechanics model was proposed in [49] to determine the effective stress intensity factor amplitude to propagate crack in CNT-based PNC, under the assumption that the crack-opening displacement at a distance behind the crack tip equals the pull-out length, leading to Equation (5.74),

$$\Delta K_1^{\text{eff}} = \sqrt{\Delta K_1^2 - \frac{2G\rho w_c}{(1-v)\beta}}, \quad (5.74)$$

where ΔK_1 is the stress intensity factor amplitude in the absence of bridging, w_c is the work required to pull out a single nanotube, ρ is the number density of CNT penetrating the plane of the crack and β ($\beta > 1$) is a parameter accounting for the number of fibres contributing to toughening, since not all fibres penetrating crack plane participate in the bridging process.

Modelling of fracture in PNC is motivated by the fact that cracking is accompanied by bridging action of nanofillers, such as CNT [50]. Basically, in the idealisation of crack bridging, it is assumed that embedded nanotubes in a polymer matrix align perpendicular to the crack front in the matrix to provide resistance to crack propagation (Figure 5.8). In this context, the objective of fracture modelling in PNC is to relate the fracture energy of PNC to the nanoscale mechanical properties of the nanotube and the nanotube-polymer interface. Analytically, cohesive zone model is an effective approach to characterise the fracture properties of nanotube-polymer interface, as applied in [50], where a shear opening model was derived based on cohesive zone potential leading to Equation (5.75).

$$F_{\max} = \frac{4\pi}{\sqrt{2e}} RL \frac{\Gamma_I}{\delta_{cr}} \quad (5.75)$$

where $F_{\max}$ represents the maximum force at which shear opening occurs at the interface, R and L are the nanotube outer radius and embedded length, respectively, Γ_I is the intrinsic fracture energy of the interface, and δ_{cr} is the critical crack opening displacement of the interface. According to [50], a good model for fracture energy should be able to correctly quantify the contribution of interfacial adhesion between the nanotube and polymer, and at high velocities of nanotube pull-out, viscous dissipation of the polymer up to the time of pull-out must be accounted for, as the pull-out force is dependent on the velocity.

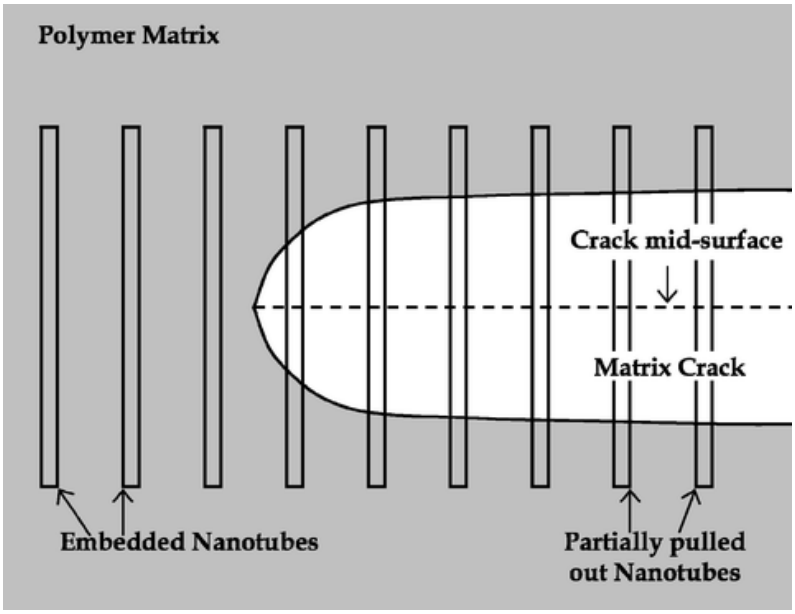

Figure 5.8: Schematic of crack bridging mechanism of carbon nanotube [50].

In general, to describe yielding or fracture behaviour of nanocomposites, detail atomistic observations involving chemical bond breaking must be accounted for [51]. Therefore, application of macroscopic or continuum modelling is limited in this context. For nanocomposites with hollow or filled nanotubes or nanowires, whose shapes resemble macroscopic thin-walled hollow columns or tubes, failure criteria can be described analogously to macroscopic conditions. As such, a multiscale approach may be an effective means to characterise fracture in these nanocomposites, considering the computational efficiency of macroscale methods and accuracy of atomistic modelling. An example of multiscale method, which combined continuum mechanics with molecular dynamics to describe atomistic prediction of failure in CNT-based nanocomposites has been presented in [51].

A CNT system under biaxial tensile-torsional loads was modelled using MD technique in which short covalent interactions are characterised with the aid of many-body and reactive empirical bond-order (REBO) potentials. Moreover, long range van der Waals interactions are captured in the form of Lennard-Jones potential. The CNT system, which is fixed at one end and subjected to applied biaxial tension-torsion at the other end, is subjected to incremental load to obtain the load paths (Figure 5.9). The stresses experienced by the CNTs were calculated by continuum mechanics approach which considers the CNTs as geometrically equivalent to macroscopic thin-walled columns or tubes. The calculated stresses are finally transformed to the principal stresses to determine the failure criteria.

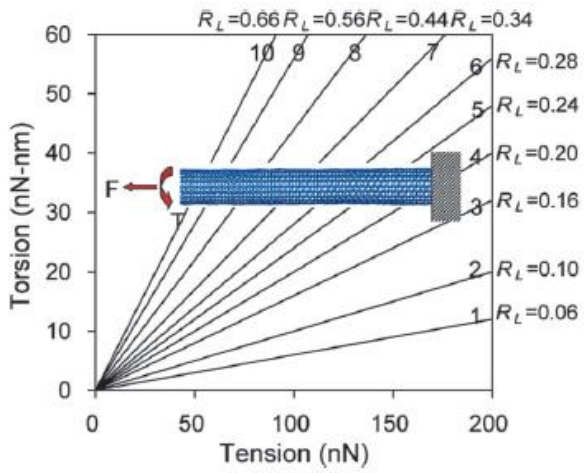

Figure 5.9: Loading paths for MD simulations of CNT under biaxial tension-torsion for different combinations of tension/torsion ratio (R_L) [51].

In particle-filled nanocomposites, depending on the nature of load, fracture may occur inter-grain in the embedding matrix. In such case, a method that provides quantum mechanical description of the interactions is suggested to study the onset of fracture accurately, as demonstrated in [52], where tight-binding MD method was used to investigate the fracture properties of tetrahedral amorphous carbon and nanodiamond-filled composites.

5.3.4 Creep

Modelling creep behaviour of materials is important, because creep failure occurs at a stress lower than the yielding stress of the material. Since creep is a time-dependent plastic deformation over a long period of loading (Figure 5.10), viscoelasticity of the polymer matrix plays an important role and hence must be considered. Classically, the viscoelastic creep model known as Burgers model (or four-element model) and empirical model named Findley model have been widely applied to PNCs [53]. However, these models are limited in application, considering the effect of elastic properties of nanocomposite constituents. Based on the principle of elastic-viscoelastic correspondence, an empirical formula for the creep strain of nanocomposites was proposed in [54] as

$$\varepsilon_{\mathrm{nc}}(t,\bar{\sigma},T)=\frac{\bar{\sigma}}{\mathrm{f}\left(E_f,\left(S_{\mathrm{m_{exp}}}(t,\bar{\sigma},T)\left(\frac{S_{\mathrm{m_{exp}}}(t_0,\bar{\sigma},T)}{S_{\mathrm{m_{exp}}}(t,\bar{\sigma},T)}\right)^{\left(V_f k_c\right)}\right),V_f,r_e\right)} \quad (5.76)$$

where $S_{\mathrm{m}_{\mathrm{exp}}}$ represents the time-varying creep stiffness of the pure matrix, $\bar{\sigma}$ is applied stress and T is the temperature. In addition, r_e is the exfoliation ratio, E_f is the elastic modulus of the nanofiller, while k_c represents the constraint factor which accounts for constraints imposed by the nanofillers on the movement of long chains and the molecule of the polymer.

In terms of micromechanical approach, a realistic prediction of the creep performance of nanotube-based composites must consider the elastic properties of the nanotube, the viscoelastic attributes of the interface and the state of dispersion of the nanotubes in the polymer matrix [55]. In some cases, due to fabrication processes of the nanocomposites, it is essential to incorporate CNT agglomeration phenomena, such that the representative nanocomposite system is constituted by two fields: (i) pure matrix without CNT and (ii) spherical inclusions containing CNT and rest of the matrix material (Figure 5.11). In this way, the elastic stiffness of the randomly dispersed CNT-reinforced polymer nanocomposite can be described by the Eshelby principle [55]. Subsequently, the nanocomposite creep function is related to the CNT-polymer nanocomposite elastic stiffness tensor in the transform domain based on simplified unit cell model.

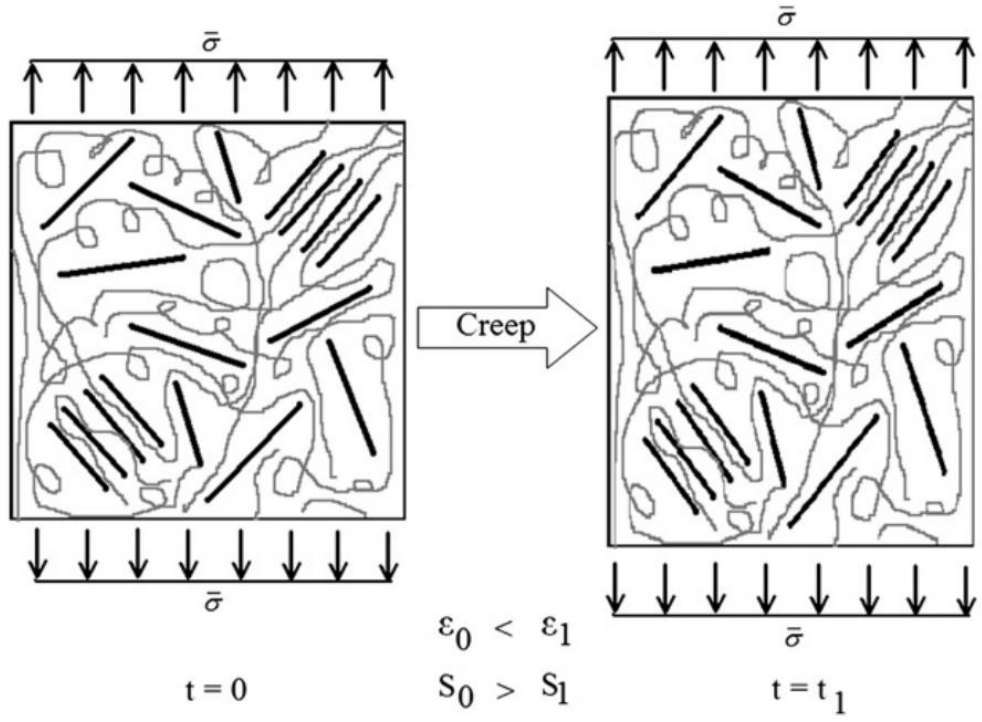

Figure 5.10: Creep mechanism in PNC [54].

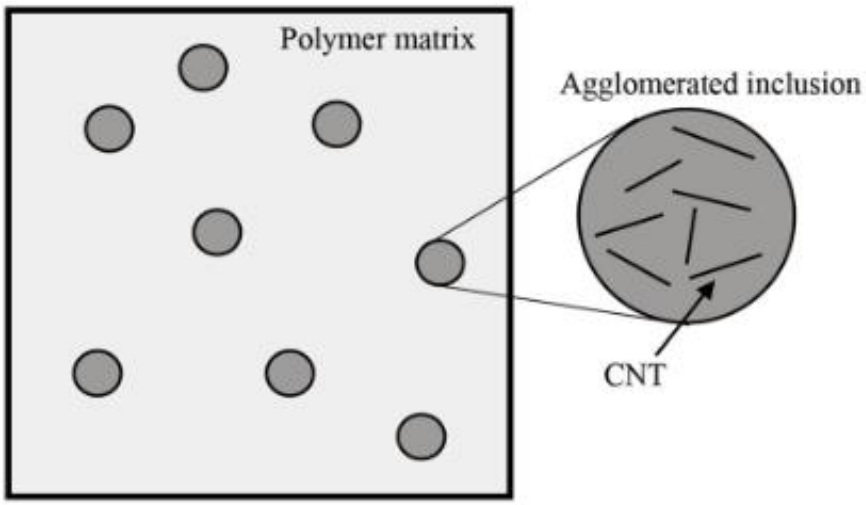

Figure 5.11: Representative system for CNT-based nanocomposites [54].

5.4 Challenges and Future Prospects

Simulating the behaviours of polymeric nanocomposites is a complex task which requires good understanding of nanoparticle structure (specifically, the effects of nanofiller size and architecture on the nanocomposite morphology), dynamics (that is, the effect of nanofiller on the rheological characteristics of the melt), solid-state properties, and processing methods and conditions. In addition, achieving optimal dispersion of nanoparticles in PNC is challenging owing to the tendency of nanophase constituents to form nanoparticle aggregates and platelet stacks or due to uncertainties in the properties of nanoparticles and dissimilarity between the chemical properties of matrix and nanofillers. In this context, theoretical models for PNC need to capture different phenomena based on realistic assumption to generate accurate predictions. Considering the structure of a PNC system with length scales up to six orders of magnitudes or time scales spanning a dozen orders of magnitude, application of analytical and numerical models at different independent scales is limited. This limitation is due to the impracticability of a single model to explore the wide length scales and time scales structurally and efficiently. As a result, modelling of PNCs demands bridging of different length and time scales through combined computational methods that can simulate fundamental molecular processes and seamlessly transfer numerical parameters efficiently across wide scales to satisfactorily predict bulk properties of PNC structures.

It is important to elucidate that availability, reliability and accuracy of experimental data are challenges that significantly influence the performance of theoretical models for prediction of PNC behaviours. These challenges increase with the advent of more innovative PNCs through

introduction of new bio-nanofillers and/or nanoparticles, especially from agricultural wastes. Therefore, robust computational schemes, with capabilities for design, optimisation, and characterisation, are required to adequately explore the merits of PNC materials for enhanced engineering applications. As the challenges in the field of PNCs evolve rapidly within the thriving field of composite science and technology, especially in the next decade, computational modelling of PNCs will remain one of the most active fields in the nearest future.

5.5 Concluding Remarks

Various theoretical models and methods/approaches have been extensively described with respect to the computational approaches to PNCs within this comprehensive chapter. It is evident that nanoparticles improve both properties and applications of several PNCs. From the multiscale perspective, computational modelling of PNCs involves three approaches, depending on the structural levels: molecular, micro and meso/macroscale. These approaches are generally classified into analytical and numerical methods. In addition, these approaches are applicable at different length, time scales and levels of complexity. Towards enhancing the properties of PNCs for high-technology applications, structural characterisation, and precise manipulation of the fabrication of the nanostructured materials must be achieved. This implies that the nanocomposite structure as well as physical and chemical processes at the nanoscale level must be correctly characterised to control the final properties of PNCs. In this context, adaptable modelling strategies (using analytical and numerical computational tools) combined with advanced experimental techniques are required to effectively explore the design of PNC structures for optimised performances.

References

[1] Zeng, Q., & Yu, A. (2010). Prediction of the Mechanical Properties of Nanocomposites. Optimisation of Polymer Nanocomposite Properties, 301–331. Available at https://doi.org/10.1002/9783527629275.ch14.

[2] Zeng, Q. H., Yu, A. B., & Lu, G. Q. (2008). Multiscale modelling and simulation of polymer nanocomposites. Progress in Polymer Science, 33(2), 191–269.

[3] Loos, M. (2015). Fundamentals of Polymer Matrix Composites Containing CNTs. Carbon Nanotube Reinforced Composites, 125–170. Available at https://doi.org/10.1016/B978-1-4557-3195-4.00005-9.

[4] Zhao, S., Zhao, Z., Yang, Z., Ke, L., Kitipornchai, S., & Yang, J. (2020). Functionally graded graphene reinforced composite structures: A review. Engineering Structures, 210, 110339.

[5] Hosford, W. R. (2013). Elementary Materials Science. Chapter 10. Available at https://www.asminternational.org/documents/10192/1849770/5373G_TOC.pdf.

[6] Luo, Z., Li, X., Shang, J., Zhu, H., & Fang, D. (2018). Modified rule of mixtures and Halpin-Tsai model for prediction of tensile strength of micron-sized reinforced composites and Young's modulus of multiscale reinforced composites for direct extrusion fabrication. Advances in Mechanical Engineering, 10(7), 1-10.

[7] Tandon, G. P., & Weng, G. J. (1984). The effect of aspect ratio of inclusions on the elastic properties of unidirectionally aligned composites. Polymer Composites, 5(4), 327-333.

[8] Lin, W. (2013). Modelling of thermal conductivity of polymer nanocomposites. Modelling and Prediction of Polymer Nanocomposite Properties, 169-200.

[9] Clancy, T. C., Frankland, S. J. V., Hinkley, J. A., & Gates, T. S. (2010). Multiscale modelling of thermal conductivity of polymer/carbon nanocomposites. International Journal of Thermal Sciences, 49(9), 1555-1560.

[10] Safi, M., Hassanzadeh-Aghdam, M. K., & Mahmoodi, M. J. (2020). A semi-empirical model for thermal conductivity of polymer nanocomposites containing carbon nanotubes. Polymer Bulletin, 77(12), 6577-6590.

[11] Guthy, C., Du, F., Brand, S., Winey, K. I., & Fischer, J. E. (2007). Thermal conductivity of single-walled carbon nanotube/PMMA nanocomposites. Journal of Heat Transfer, 129(8), 1096-1099.

[12] Benveniste, Y., & Miloh, T. (1986). The effective conductivity of composites with imperfect thermal contact at constituent interfaces. International Journal of Engineering Science, 24(9), 1537-1552.

[13] Hasselman, D. P. H., & Johnson, L. F. (1987). Effective thermal conductivity of composites with interfacial thermal barrier resistance. Journal of Composite Materials, 21(6), 508-515.

[14] Russell, H. W. (1935). Principles of heat flow in porous insulators. Journal of the American Ceramic Society, 18(1-12), 1-5.

[15] Tsao, G. T. N. (1961). Thermal conductivity of two-phase materials. Industrial & Engineering Chemistry, 53(5), 395-397.

[16] Cheng, S. C., & Vachon, R. I. (1969). The prediction of the thermal conductivity of two and three phase solid heterogeneous mixtures. International Journal of Heat and Mass Transfer, 12(3), 249-264.

[17] Maxwell, J. C. (1873). A treatise on electricity and magnetism (Vol. 1). Clarendon press.

[18] Fricke, H. (1924). A mathematical treatment of the electric conductivity and capacity of disperse systems I. The electric conductivity of a suspension of homogeneous spheroids. Physical Review, 24(5), 575-587.

[19] Hamilton, R. L., & Crosser, O. K. (1962). Thermal conductivity of heterogeneous two-component systems. Industrial & Engineering chemistry fundamentals, 1(3), 187-191.

[20] Hashin, Z. (1968). Assessment of the self consistent scheme approximation: conductivity of particulate composites. Journal of Composite Materials, 2(3), 284-300.

[21] Allen, M. P., & Tildesley, D. J. (2017). Computer Simulation of Liquids. Oxford University Press.

[22] Frenkel, D., & Smit, B. (2001). Understanding Molecular Simulation: From Algorithms to Applications, Vol. 1, Elsevier: UK.

[23] Kwon, Y. W. (2015). Molecular Dynamics. Multiphysics and Multiscale Modelling, 145–186. doi:10.1201/b19098-5.

[24] Schneider R., Sharma A.R., Rai A. (2008). Introduction to Molecular Dynamics. In: Fehske H., Schneider R., Weiße A. (eds) Computational Many-Particle Physics. Lecture Notes in Physics, Vol. 739. Springer, Berlin, Heidelberg. Available at https://doi.org/10.1007/978-3-540-74686-7_1.

[25] Raychaudhuri, S. (2008, December). Introduction to monte carlo simulation. In 2008 Winter simulation conference (pp. 91-100). IEEE.

[26] Odegard, G. M., Gates, T. S., Wise, K. E., Park, C., & Siochi, E. J. (2003). Constitutive modelling of nanotube–reinforced polymer composites. Composites science and technology, 63(11), 1671-1687.

[27] Doi, M. (2002). Octa - A Free and Open Platform and Software of Multiscale Simulation for Soft Materials.

[28] Müller-Plathe, F. (2002). Coarse-graining in polymer simulation: From the atomistic to the mesoscopic scale and back. ChemPhysChem, 3(9), 754-769.

[29] Toth, R., Voorn, D. J., Handgraaf, J. W., Fraaije, J. G., Fermeglia, M., Pricl, S., & Posocco, P. (2009). Multiscale computer simulation studies of water-based montmorillonite/poly (ethylene oxide) nanocomposites. Macromolecules, 42(21), 8260-8270.

[30] Kasemägi, H., Klintenberg, M., Aabloo, A., & Thomas, J. O. (2002). Molecular dynamics simulation of the $LiBF_4$–PEO system containing Al2O3 nanoparticles. Solid State Ionics, 147(3-4), 367-375.

[31] Spanos, P. D., & Kontsos, A. (2008). A multiscale Monte Carlo finite element method for determining mechanical properties of polymer nanocomposites. Probabilistic Engineering Mechanics, 23(4), 456-470.

[32] Kontsos, A., & Spanos, P. D. (2009). Modelling of nanoindentation data and characterisation of polymer nanocomposites by a multiscale stochastic finite element method. Journal of Computational and Theoretical Nanoscience, 6(10), 2273-2282.

[33] Kontsos, A., & Cuadra, J. A. (2013). Multiscale stochastic finite elements modelling of polymer nanocomposites. Modelling and prediction of polymer nanocomposite properties, 143-168.

[34] Ostoja-Starzewski, M. (2006). Material spatial randomness: From statistical to representative volume element. Probabilistic engineering mechanics, 21(2), 112-132.

[35] Swaminathan, S., Ghosh, S., & Pagano, N. J. (2006). Statistically equivalent representative volume elements for unidirectional composite microstructures: Part I-Without damage. Journal of Composite Materials, 40(7), 583-604.

[36] Shi, D. L., Feng, X. Q., Huang, Y. Y., Hwang, K. C., & Gao, H. (2004). The effect of nanotube waviness and agglomeration on the elastic property of carbon nanotube-reinforced composites. Journal of Engineering Materials and Technology, 126(3), 250-257.

[37] Zheng, X., Forest, M. G., Lipton, R., & Zhou, R. (2007). Nematic polymer mechanics: flow-induced anisotropy. Continuum Mechanics and Thermodynamics, 18(7), 377-394.

[38] Lee, K. Y., & Paul, D. R. (2005). A model for composites containing three-dimensional ellipsoidal inclusions. Polymer, 46(21), 9064-9080.

[39] Wagner, H. D. (2002). Nanotube–polymer adhesion: a mechanics approach. Chemical Physics Letters, 361(1-2), 57-61.

[40] Mokashi, V. V., Qian, D., & Liu, Y. (2007). A study on the tensile response and fracture in carbon nanotube-based composites using molecular mechanics. Composites Science and Technology, 67(3-4), 530-540.

[41] Fisher, F. T., Bradshaw, R. D., & Brinson, L. C. (2003). Fibre waviness in nanotube-reinforced polymer composites—I: Modulus predictions using effective nanotube properties. Composites Science and Technology, 63(11), 1689-1703.

[42] Bradshaw, R. D., Fisher, F. T., & Brinson, L. C. (2003). Fibre waviness in nanotube-reinforced polymer composites - II: Modelling via numerical approximation of the dilute strain concentration tensor. Composites Science and Technology, 63(11), 1705-1722.

[43] Ashrafi, B., & Hubert, P. (2006). Modelling the elastic properties of carbon nanotube array/polymer composites. Composites Science and Technology, 66(3-4), 387-396.

[44] Hbaieb, K., Wang, Q. X., Chia, Y. H. J., & Cotterell, B. (2007). Modelling stiffness of polymer/clay nanocomposites. Polymer, 48(3), 901-909.

[45] Zare, Y., Fasihi, M., & Rhee, K. Y. (2017). Efficiency of stress transfer between polymer matrix and nanoplatelets in clay/polymer nanocomposites. Applied Clay Science, 143, 265-272.

[46] Frankland, S. J. V., Caglar, A., Brenner, D. W., & Griebel, M. (2002). Molecular simulation of the influence of chemical cross-links on the shear strength of carbon nanotube - polymer interfaces. The Journal of Physical Chemistry B, 106(12), 3046-3048.

[47] Wong, M., Paramsothy, M., Xu, X. J., Ren, Y., Li, S., & Liao, K. (2003). Physical interactions at carbon nanotube-polymer interface. Polymer, 44(25), 7757-7764.

[48] Li, C., & Chou, T. W. (2003). Multiscale modelling of carbon nanotube reinforced polymer composites. Journal of Nanoscience and Nanotechnology, 3(5), 423-430.

[49] Zhang, W., Picu, R. C., & Koratkar, N. (2007). Suppression of fatigue crack growth in carbon nanotube composites. Applied Physics Letters, 91(19), 1-4.

[50] Seshadri, M., & Saigal, S. (2007). Crack bridging in polymer nanocomposites. Journal of Engineering Mechanics, 133(8), 911-918.

[51] Jeong, B. W., Lim, J. K., & Sinnott, S. B. (2007). Multiscale-failure criteria of carbon nanotube systems under biaxial tension–torsion. Nanotechnology, 18(48), 1-7.

[52] Fyta, M. G., Remediakis, I. N., Kelires, P. C., & Papaconstantopoulos, D. A. (2006). Insights into the fracture mechanisms and strength of amorphous and nanocomposite carbon. Physical Review Letters, 96(18), 1-4.

[53] Yang, J. L., Zhang, Z., Schlarb, A. K., & Friedrich, K. (2006). On the characterisation of tensile creep resistance of polyamide 66 nanocomposites. Part II: Modelling and prediction of long-term performance. Polymer, 47(19), 6745-6758.

[54] Shokuhfar, A., Zare-Shahabadi, A., Atai, A. A., Ebrahimi-Nejad, S., & Termeh, M. (2012). Predictive modelling of creep in polymer/layered silicate nanocomposites. Polymer Testing, 31(2), 345-354.

[55] Hassanzadeh-Aghdam, M. K., Mahmoodi, M. J., & Ansari, R. (2019). Creep performance of CNT polymer nanocomposites-An emphasis on viscoelastic interphase and CNT agglomeration. Composites Part B: Engineering, 168, 274-281.